

Summer project Interact 2015

Theodor S. Holstad*
Summer student, Sintef Energy
 (Dated: August 12, 2015)

In this project, a ground heat exchanger system (GHE) has been simulated using the Modelica language in the Dymola environment. This GHE is a component that later is to be incorporated into a larger system. It is therefore desired to use a complex model of the GHE to produce a simple model that can be used in a larger system. In this manner, the computation time in the larger system can be greatly reduced. A B2G model was used, because this produced much more accurate results during short-term simulations, which often are of interest in control systems ([1], [2], [3]).

Introduction

Ground coupled heat systems (GHE) consisting of vertical boreholes drilled into the ground can contribute to reduce consumption of primary energy all around the world. It is therefore an important contribution to reduce emissions of CO₂ and hence the undesirable impacts such as constumtion has on the environment. The system's primary function is to provide heating and cooling to buildings, and it may be incorporated as a component into a larger system consisting of several other units.

The BHE model used in this work is the Borehole-to-Ground (B2G) model, which has been developed at the Universitat Politcnica de Valencia [2].

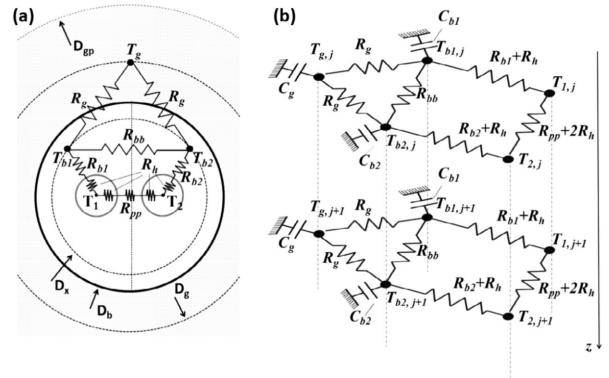


FIG. 1: Model of the boreHoleSegment cross section.

Experimental setup of model

Description

The model consists of three types of entities:

- **Buildingblocks:** the basic units that are used to construct larger components.
- **Components:** these are more complex entities that are constructed from buildingblocks.
- **Testers:** these are codes that simulate the components interacting together and set up the overall environment for a simulation.

Buildingblocks

The most basic building block in the model is the boreHoleSegments. These are tranverse intersections of the boreHole itself. In order to build this component, the B2G model was used. The abstract representation of such a cross section can be seen in figure 1 and the implemented version in Dymola in figure 2. The boreHoleSegment is circular and there are two smaller circular pipes inside of it. The borehole is filled with water, while the pipes are filled with an aqueous solution of 20 volume percent ethanol. In Dymola, the two pipes are represented with two pipe elements, as seen in figure 2.

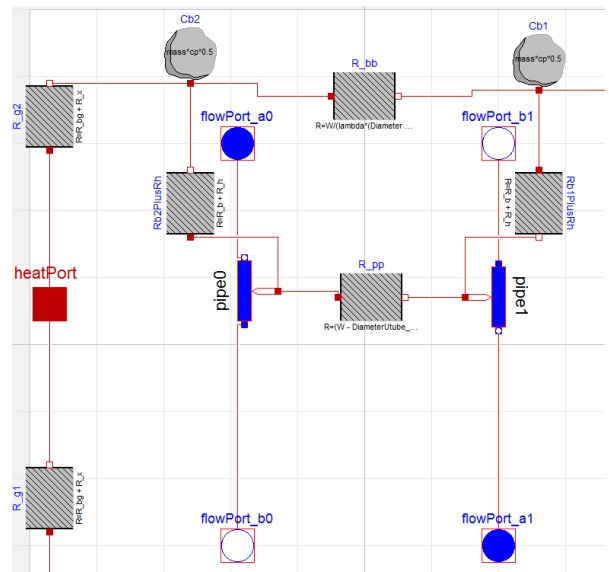


FIG. 2: Model of the boreHoleSegment cross section in Dymola.

Components

In order to represent the entire borehole, several boreHoleSegment buildingblocks are connected together in the boreHole component. Each segment has a connection between its pipe_0 and the pipe_0 of the next element (downward flow), and likewise with the pipe_1's (upward flow). The lowest segment has a connection be-

the boreHoles are located in the middle of the ground-Segment, and not close to the edges, to avoid edge effects as much as possible.

Each boreHoleSegment k has its heatPort connected to element k of the heatport array heatPort of the boreHole it is a part of, as described earlier. Element k in this array is again connected to the heatPort_ext array element (i, j, k) in the groundSegment component to establish a connection between the boreHole and the ground it is embedded into. Also note in figure 8 that flowPort a_0 in the boreHole component is connected to the circulation pump and flowport b_1 in the boreHole component is connected to the outside pipe element, as mentioned earlier. This is the case for all of the boreHoles in the boreHole array, and they are thus connected in parallel. Also note that most of the parameters necessary to use in the buildingblocks, such as the resistance values, are calculated in the tester and then passed down to the buildingblocks. This is to avoid doing the computations several times in each buildingblocks, because the resistance values are the same. Also, a lot of parameters are not sent down at all, because they are not needed on the buildingblock level (e.g. Reynold's number, Prusselt's number, Prandtl's number etc.).

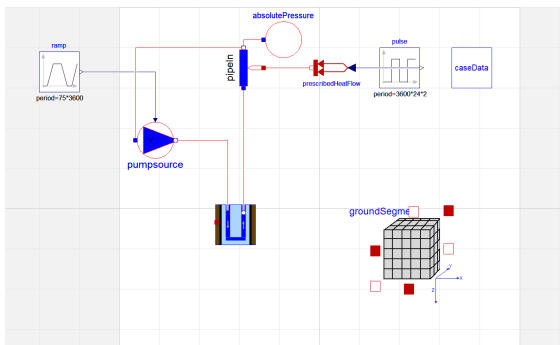


FIG. 7: Overview of the simulation setup.

```

for i in 1:caseData.nWell loop
  for j in 1:caseData.nPipe loop
    for k in 1:caseData.nBoreHole loop
      connect(boreHole[i-1]*caseData.nWell+1, heatPort[k], groundSegment.heatPort_ext[caseData.nPipe*(i-1)+caseData.nWell*k]);
      connect(pumpsource.flowPort_b, boreHole[i-1]*caseData.nWell+1, flowPort_a0);
      connect(boreHole[(i-1)*caseData.nWell+1].flowPort_b1, pipeIn.flowPort_a);
    end for;
  end for;
end for;
// Connecting the boreHoles in parallel.
connect(trapezoid.y, pumpsource.volumeFlow);
connect(pipeIn.heatPort, prescribedFlow.port);
connect(pumpsource.flowPort_a, pipeIn.flowPort_b);
connect(pipeIn.flowPort_b, absolutePressure.flowPort);
connect(pipe.y, prescribedHeatFlow.Q_flow);
a;

```

FIG. 8: Code for connecting the components in figure 7 together.

```

parameter Integer nxStart = integer(floor(0.5*(caseData.nx - (caseData.nWell + caseData.nPipe*(caseData.nWell-1)) + 1));
parameter Integer nyStart = integer(floor(0.5*(caseData.ny - (caseData.nWell + caseData.nPipe*(caseData.nWell-1)) + 1));

```

FIG. 9: Start position in x- and y-directions for first boreHole in the groundSegment.

Plotting

In order to make an animation of the simulation, the temperatures of the Tnodes are logged and saved to file every plotTimeStep. Averaging between the Tnodes are used to get extra points on the faces of the Tnodes and thus increase the resolution. These plots are collected from the xy-plane at z_plot, from the yz-plane at x_plot and from the xz-plane at y_plot. Note that in order to produce an animation, the GroundSegment_FastPlotExtraPointsXYZ_animate needs to be used instead of GroundSegment_Fast. Also, note that the simulation time is severely increased when this feature is enabled. See figure 10 for a demonstration of this feature.



FIG. 10: Animation of the xy-plane, xz-plane and yz-plane for a 9x11x6 array with 2x3 boreHoles (boreHoleArray_ComplexModel_ComplexModel_Array_Tprofile). The ground has the initial temperature profile from 16 and each boreHole is heated up by 9 kW.

Parameter values

The different resistances and capacitances presented here can be seen in figures 1 and 2. Each pipe contains a mass given by

$$m = \pi \cdot r_{\text{pipe,inner}}^2 \cdot dz \cdot \rho_{\text{ethanol-water solution}}, \quad (2)$$

where dz is the height of each pipe segment.

The capacitance of the water in the borehole segments, excluding the pipes, is distributed in the capacitances C_{b1} and C_{b2} , and is calculated as

$$c_{b1} = c_{b2} = \frac{1}{2} (dz \cdot \pi \cdot \rho \cdot (r_{\text{borehole}}^2 - 2 \cdot r_{\text{pipe,outer}}^2)), \quad (3)$$

based on equation (9) in [1].

The resistance between the two pipes, one leading water up and the other down, in each segment, is calculated as

$$R_{pp} = \frac{W - D_{\text{pipe,outer}}}{D_{\text{pipe,outer}} \cdot dz \cdot k_b} \quad (4)$$

based on equation (18) in [1].

The resistance between the two capacitances C_{b1} and C_{b2} is

$$R_{bb} = \frac{W}{k_b \cdot (D_{\text{borehole}} - D_{\text{pipe,outer}}) \cdot dz} \quad (5)$$

based on equation (19) in [1].

The resistance between the pipes and the capacitances C_{b1} and C_{b2} , is calculated as

$$R_{pipesToWater} = R_h + R_b \quad (6)$$

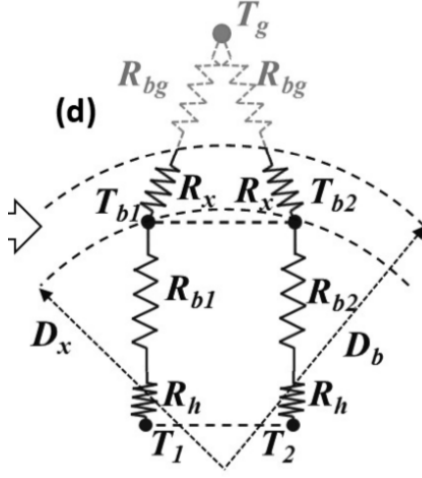


FIG. 11: Figure 3 d) in [1].

based on figure 11. Here, R_b is a conductive resistance given by

$$R_{b1} = R_{b2} = R_b = \frac{\ln\left(\frac{D_x}{D_{eq}}\right)}{\pi \cdot k_b \cdot dz} \quad (7)$$

(equation 16, [1]), where k_b is the borehole conductivity, which is equal to the conductivity of water as it is filled with water (according to [5], most boreholes in Sweden are filled with water, in particular the one that is used to confirm this model). D_{eq} is an equivalent surface to the surface of the two pipes, as shown in figure 12 a).

$$D_{eq} = D_{pipe,outer} \cdot \sqrt{\frac{4W}{\pi D_{pipe,outer}} + 1} \quad (8)$$

(equation (15) in [1]).

According to figure 1 a), if r_x is the radial position of the capacitances C_{b1} and C_{b2} , $D_x = 2r_x$ is the diameter of the circle intersecting them. At first, the radial position r_x was chosen as the center of mass of a semi-circular disk. This seemed natural, because the borehole is split into *two* capacitance nodes. If we align r' along the x-axis,

$$D_x = 2r_x = 2 \frac{\int_{-\frac{\pi}{2}}^{\frac{\pi}{2}} \int_0^{r_{borehole}} \rho(r' \cos(\theta)) r' dr' d\phi}{\frac{1}{2} \cdot \rho \pi r_{borehole}^2} = \frac{8r_{borehole}}{3\pi}. \quad (9)$$

However, this turned out to not be a good approximation, since according to [1], $D_{eq} < D_x < D_{borehole}$, and it is there concluded that $D_x = D_{borehole}$ actually gives the best approximation. Thus,

$$D_x = D_{borehole} \quad (10)$$

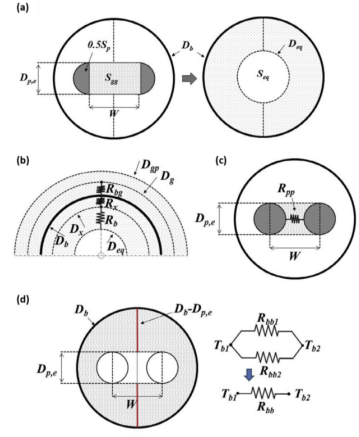


Fig. 4. Geometrical model characteristics to calculate (a) the equivalent diameter [33], (b) gross nodes position, (c) pipe to pipe thermal resistance, and (d) gross node to gross node thermal resistance.

FIG. 12: Figure 4 in [1].

was chosen. R_h is the convective resistance of the water inside the pipes, and it is given by

$$R_h = \frac{1}{\pi \cdot dz \cdot \text{Nu} \cdot k} \quad (11)$$

(equation (13), [1]), where Nu is the Nusselt number and k is the conductivity of the medium inside the pipe, an aqueous ethanol solution. For a circular pipe, the Nusselt number is given by

$$\text{Nu}_{\text{Laminar}} = \frac{3.657}{\tanh(2.264X^{\frac{1}{3}} + 1.7X^{\frac{2}{3}})} + \frac{0.0499}{X} \tanh(X), \quad (12)$$

(equation (54) in section B1 in [4]), and

$$\text{Nu}_{\text{Turbulent}} = 0.024 \cdot \text{Reynold}^{0.8} \cdot \text{Prandtl}^{\frac{1}{3}} \quad (13)$$

(equation (56) in section B1 in [4]), where

$$X = \frac{dz}{D_{pipe,inner} \cdot \text{Reynold} \cdot \text{Prandtl}}. \quad (14)$$

Furthermore, Reynold's number for flow in a circular pipe is given by

$$\text{Reynold} = \frac{w \cdot D_{pipe,inner}}{\nu}, \quad (15)$$

(equation (10) section B1 in [4]). Note that the diameter of the pipe is the characteristic length L . w is the water velocity in the pipes, given by

$$w = \frac{\dot{V}}{\pi \cdot r_{pipe,inner}^2}, \quad (16)$$

where \dot{V} is the volume flow rate through the pipes. ν is the kinematic viscosity of the medium (water). The Prandtl number is given by

$$\text{Prandtl} = \frac{\nu \cdot \rho \cdot c_p}{k_{\text{water}}}, \quad (17)$$

according to (12) in section B1 of [4].

Furthermore, the fraction of laminar flow is denoted by x , where

$$x = \begin{cases} 1 & \text{if Reynold} < 2300. \\ \frac{10000 - \text{Reynold}}{10000 - 2300} & \text{if } 2300 < \text{Reynold} < 10000. \\ 0 & \text{if Reynold} > 10000. \end{cases} \quad (18)$$

based on the fact that fluid flow in pipes is laminar if $\text{Reynold} < 2300$, mixed if $2300 < \text{Reynold} < 10000$, and turbulent if $\text{Reynold} > 10000$ (based on [4], section B1, page 25).

Then, finally

$$\text{Nu} = x \cdot \text{Nu}_{\text{Laminar}} + (1 - x) \cdot \text{Nu}_{\text{Turbulent}}. \quad (19)$$

Next, the pressure losses were calculated. The pipe component has two pressure losses: dpLaminar and dpNominal for laminar and turbulent flow respectively. According to [4] section L1.2, the pressure loss of a medium flowing in a circular pipe is

$$\Delta p = \zeta \frac{dz}{D_{\text{pipe,inner}}} \frac{\rho w^2}{2} = \zeta \frac{dz}{D_{\text{pipe,inner}}} \frac{\rho \dot{V}^2}{2 \cdot \pi^2 \cdot r_{\text{pipe,inner}}^4} \quad (20)$$

where

$$\zeta_{\text{Laminar}} = \frac{64}{\text{Reynold}}, \quad (21)$$

and

$$\zeta_{\text{Turbulent}} = \frac{0.3164}{\text{Reynold}^{\frac{1}{4}}}. \quad (22)$$

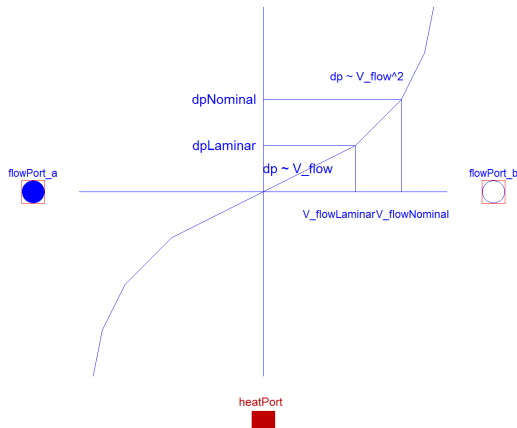


FIG. 13: Descriptive picture of the Modelica heated pipe component.

As can be seen in the modelica pipe component in figure 13, $V_{\text{flowLaminar}}$ (henceforth denoted \dot{V}_{laminar}) and

$V_{\text{flowNominal}}$ (henceforth denoted $\dot{V}_{\text{Turbulent}}$) are the flow rates at which the flow in the pipe goes from laminar to mixed and mixed to turbulent, respectively. In our case, since from (15) and (16)

$$\text{Reynold} = \frac{\dot{V} \cdot D_{\text{pipe,inner}}}{\nu \cdot \pi \cdot r_{\text{pipe,inner}}^2} = \frac{4\dot{V}}{\nu \cdot \pi \cdot D_{\text{pipe,inner}}}, \quad (23)$$

we have based on this and on (18)

$$\dot{V}_{\text{laminar}} = \frac{2300 \cdot \nu \cdot \pi \cdot D_{\text{pipe,inner}}}{4}, \quad (24)$$

and

$$\dot{V}_{\text{nominal}} = \frac{10000 \cdot \nu \cdot \pi \cdot D_{\text{pipe,inner}}}{4}. \quad (25)$$

Thus, combining equations (20), (21) and (22)

$$\Delta p_{\text{laminar}} = \frac{64}{2300} \frac{dz}{D_{\text{pipe,inner}}} \frac{\rho \dot{V}_{\text{laminar}}^2}{2 \cdot \pi^2 \cdot r_{\text{pipe,inner}}^4},$$

$$\Delta p_{\text{nominal}} = \frac{0.3164}{10000^{\frac{1}{4}}} \frac{dz}{D_{\text{pipe,inner}}} \frac{\rho \dot{V}_{\text{nominal}}^2}{2 \cdot \pi^2 \cdot r_{\text{pipe,inner}}^4}.$$

Finally, combining this with equations (24) and (25) gives

$$\Delta p_{\text{laminar}} = 73600 \frac{dz \rho \nu^2}{D_{\text{pipe,inner}}^3}, \quad (26)$$

$$\Delta p_{\text{nominal}} = 1582000 \frac{dz \rho \nu^2}{D_{\text{pipe,inner}}^3}. \quad (27)$$

Next, the thermal capacitance C_g of the ground as well as the thermal resistance R_g (between the water in the boreHole and the ground) both had to be computed. In [1], this is done by first defining D_{gp} as the penetration radius of the boreHole. This means the extent to which heat is stored in the surrounding soil around the boreHole. That is, how much of the surrounding soil responds in time and can thus be included in the capacitance. This obviously depends on simulation time. However, since this project is based on a dynamic model where the groundSegment nodes interact, it should not be necessary to specify such a capacitance. Each boreholeSegment is connected to a groundSegment temperature node, and can exchange heat with the capacitance element of that groundSegment. Then this groundSegment interact with the surrounding ones and so on. In addition, each boreHoleSegment has its own internal capacitances C_{b1} and C_{b2} , as can be seen in figure 2. Hence, the capacitance of the ground increases with simulation time, and is thus determined in a dynamical manner in this model. However, it does become necessary to define R_g , since it occurs in the equations of this model. Equation (22) in [1] gives

$$R_{g1} = R_{g2} = R_g = R_x + R_{bg}, \quad (28)$$

where R_x is the thermal resistance between the capacitance nodes C_{b1} and C_{b2} of the borehole and the borehole wall, given by equation (17) in [1],

$$R_x = \frac{\ln\left(\frac{D_{borehole}}{D_x}\right)}{\pi k_b dz} = 0, \quad (29)$$

(because $D_{borehole} = D_x$ in our model) and R_{bg} is the thermal resistance between the borehole wall and the surrounding ground, given by equation (21) in [1],

$$R_{bg} = \frac{1}{\pi k_g dz} \ln\left(\frac{D_g}{D_{boreHole}}\right), \quad (30)$$

where D_g is the diameter of a circle placed in the middle between the circle with diameter D_{gp} (penetration diameter) and $D_{boreHole}$ (borehole diameter), see figure 12 b). In the current model, the borehole is embedded in the same groundsegment node that it is connected to. It would therefore be logical to represent the corresponding D_g as the diameter of a circle midway between a circle tangent to the sides of the groundSegment and a circle with a diameter of the boreHole. The sidelength of the groundSegment in the x-direction is used to get the tangential circle, and it would therefore be convenient if the sidelength in the y-direction is the same to make it tangent in the y-direction as well, that is $\frac{L_x}{n_x} = \frac{L_y}{n_y}$. This is to avoid different geometries in the xz-plane and yz-plane. The formula used is thus,

$$D_g = D_{boreHole} + \frac{\frac{L_x}{n_x} - D_{boreHole}}{2}. \quad (31)$$

Note that the groundSegment obviously should be larger than the boreHole. I. e. $\frac{L_x}{n_x} = \frac{L_y}{n_y} > D_{borehole}$.

MODEL VALIDATION FOR SHORT TIMES (DAYS)

Qualitative testing

In order to confirm the short term behaviour of the model, it was necessary to confirm that it agrees to [1] when using the same parameter values. A qualitative test was done to confirm that the model behaves similarly to the B2G model.

As mentioned in [1] and [2], if the output temperature and input temperature is plotted versus time, and there is a temperature increase in the input, the B2G model correctly incorporates the time delay due to the fact that the circulating fluid needs to travel through the U-tube. As can be seen in figure 14, our model also show such a delay in the response. Also note that the pipes clearly lose heat to the surrounding groundSegment capacitances and the boreHole capacitances. This is reflected from the fact that the increase in temperature is greatest

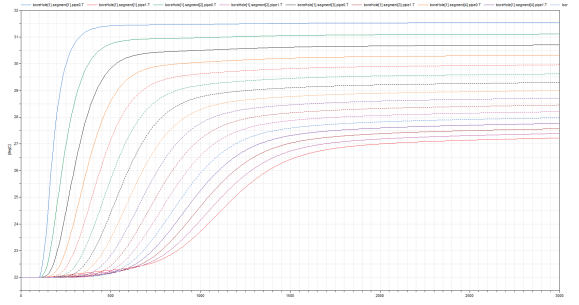


FIG. 14: Results from the first qualitative testing of the model, 10/7/2015. The temperatures of all the pipes have been plotted. The temperature is 22 degrees celsius everywhere, when the temperature pumped into the system suddenly is increased linearly.

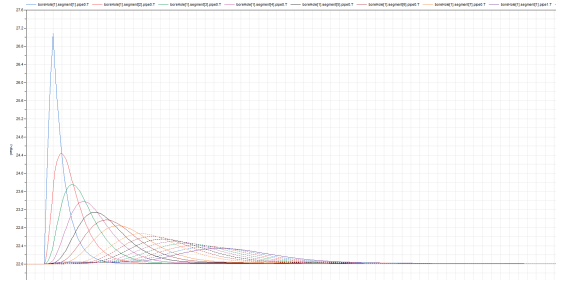


FIG. 15: Results from the second qualitative testing of the model, 10/7/2015. This time the pumped in water temperature followed an exponential pulse. A response that slowly becomes smaller due to losses to the boreHole capacitance and groundSegment capacitances can be seen, and a delay is also present in this case

at the inlet, and then becomes smaller and smaller further down the U-tube, being smallest at the outlet. Also note the linear rise in temperature at the very beginning of the simulation in the last few pipes. This is due to heat transfer through R_{pp} . The temperature of these pipes starts to increase more rapidly later when the water finally reaches them. All this can be seen in figure 14.

A similar test was done with a exponential pulse, and the result can be seen in figure 15. All these characteristics were also found in [1].

Quantitative testing

The next objective was to get quantitative agreement with [1] and [2]. To provide more information about the experimental setup, the references provided in [1] led to [5] and [6]. One of the boreholes in [6] is based on the experiment in [5].

[7] conducts a numerical analysis of the experiment in [5]. To verify the model, the results from [7] were first reproduced in Modelica. A comparison was also done to one of the results in [6].

In these experiments, distributed thermal response tests (DTRTs) are carried out. This means that the temperature is measured at different depths along the borehole while running a conventional thermal response test. A laser pulse is sent through a fiber optic cable, and the frequency shift due to Raman scattering and the time delay of the signal are used to measure the temperature and vertical position, respectively. See [5] for more information about this.

The initial undisturbed temperature distribution found in [7] can be seen in figure 16. The borehole can be seen from the side in figure 17. This temperature profile was used to initiate the temperature in the ground-Segment Tnodes, the water in the borehole and in the medium in the U-tube.

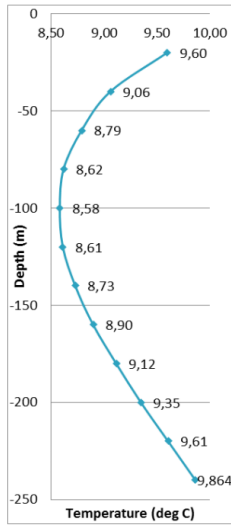


FIG. 16: Initial temperature profile from [7].

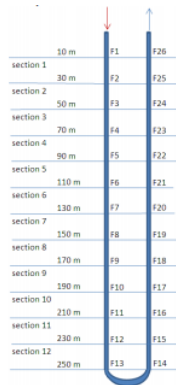


Figure 1. Borehole sectioning

FIG. 17: From [5].

The parameters used in Dymola were based on the COMSOL model in [7]. This was again based on the experimental data from [5]. The Dymola model was adjusted to have similar parameters as in that experiment:

- The borehole is 260 meters deep, and the groundwater starts 5.5 meters down in the borehole, according to [5]. In the Dymola model, a 260 meter deep borehole was used, but it might be more correct to adjust it to 254.5 meters (active depth).
- The volumetric flow rate \dot{m} was chosen to be 0.52 l/s based on [5].
- The shank spacing was not specified in [7], while in [6] it is mentioned that 78 mm is used in BHE7. In [5], it is mentioned that "The lateral position of the cable is not known, since there are no spacers or similar on the cable." $W = 78mm$ was assumed because it gave a good match with [6].
- The borehole is sectioned as in figure 17 from [5]. The Dymola model starts at the ground level and goes 260 meters down. The sections are 21.67 meters deep.
- The U-tube pipe was of type PE40x2.4 according to [5]. This pipe has an outer diameter of 40 mm and is SDR17 and thus has an inner diameter of 37.647 mm.
- Borehole diameter is 140 mm according to [5].
- The test was done by 3 days with no circulation, 1 day with circulation and no heating, 2 days of heating and circulation and then 24 hours recovery according to [7].
- The thermal conductivity of the rock was set to the optimized value in [7], $2.74W/(mK)$.
- The volumetric heat capacity of the soil was set to $\frac{2.2MJ}{m^3K}$, which is common in Scandinavia according to [9] and [10].
- The borehole was waterfilled, so the density and specific heat capacity of the water in the borehole were chosen to be equal to those of water.
- However, according to [11], the effective conductivity can increase by a factor of 3-10 due to groundwater flow. It was assumed that this factor should be around 3 in our model, because according to [6], there is little groundwater flow in the borehole, so the smallest factor of 3 was chosen.

Finally, the medium in U-tube in [7] used an aqueous solution with 20 % volume fraction ethanol. [12], section 4.4 provides graphs of thermal properties for different weight fractions and temperatures of ethanol in water. By using

$$f_{weight} = \frac{f_{volume} \cdot \rho_{ethanol}}{f_{volume} \cdot \rho_{ethanol} + (1 - f_{volume})\rho_{water}} \quad (32)$$

we find that

$$f_{weight} = \frac{0.20 \cdot 789kg/m^3}{0.20 \cdot 789kg/m^3 + (1 - 0.20)1000kg/m^3} = 0.1648 \quad (33)$$

Thus, using a weight fraction of 18.7 % at about 10 °C in table 4.4.4 (the graphs were hard to read off) gives

- $\rho = 974.1 \frac{kg}{m^3}$.
- Specific heat $c_p = 4361 \frac{J}{kgK}$
- Thermal conductivity = $0.464 \frac{W}{mK}$.
- Dynamic Viscosity = $\mu = 3.09mPa \cdot s = 3.09mN \cdot s/m^2$.
- Hence, Kinematic viscosity = $\nu = \frac{\mu}{\rho} = 3.17\mu m^2/s$.

Finally, a choice had to be made for L_x and L_y . In this simulation they were 1.55 meters, which might seem small. These are chosen by considering how much the Tnodes adjacent to the borehole respond. There should be a temperature response several Tnodes away from the borehole. Otherwise, this means that the Tnodes right next to the borehole are too big and absorb all the heat. On the other hand, the Tnodes most far away from the borehole at the edges should not respond much, to avoid edge effects. It turns out that quite small Tnodes are necessary to achieve this for simulation times of a few days, and hence L_x and L_y are quite low. On the other hand, the elements most far away have only a small temperature increase, as can be seen in figure 18, so edge effects are small and this choice should be fine. However, if the simulation time is turned up or the heat input is turned up, it might be necessary to increase L_x and L_y . Then it might also be necessary to increase n_x and n_y to keep the Tnodes small, which may increase computation time.

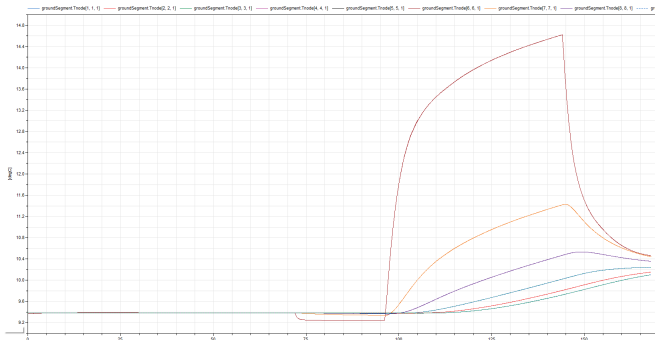


FIG. 18: Response of the Tnodes to the heat injection. Note that the ones most far away show little response. However, there is a smooth decrease, which means that the Tnodes are not too massive either.

In figures 19 and 20, the average temperature of the water in all the pipes in all the borehole segments is plotted versus time. As can be seen the figures have the same shape and agree well. Plots of the average temperature of the two pipe segments pipe0 and pipe1 for each borehole segment from Dymola and [7] are compared in the Appendix. They agree well.

In figures 21 based on BHE4 in [6] and 22 from Dymola, the average temperatures of the pipe segments pipe0 and

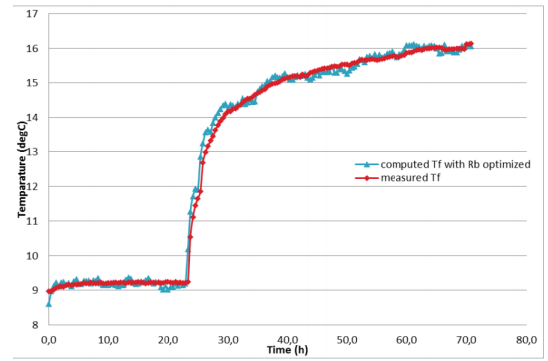


Figure 19: Computed and measured temperatures of the fluid after optimization of λ_{rock} and R_b in Section 6.

FIG. 19: Average temperature of all pipe segments as a function of simulation time in [7].

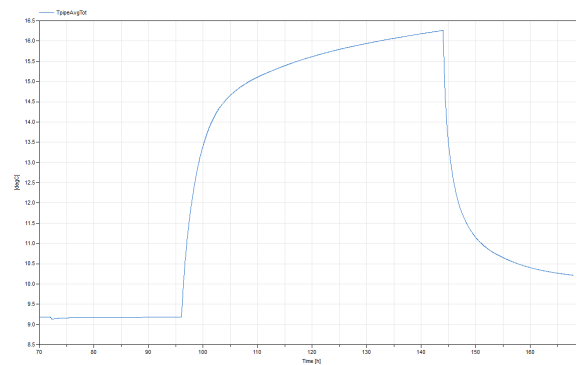


FIG. 20: Average temperature of all pipe segments as a function of simulation time in Dymola.

pipe1 for all the borehole segments are compared in one plot. They agree well.

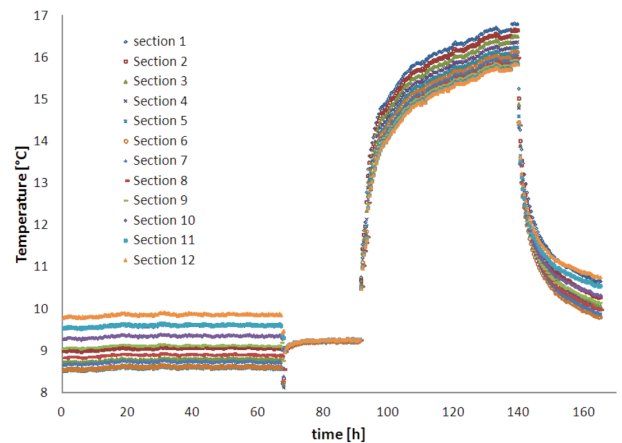


FIG. 21: From [6].

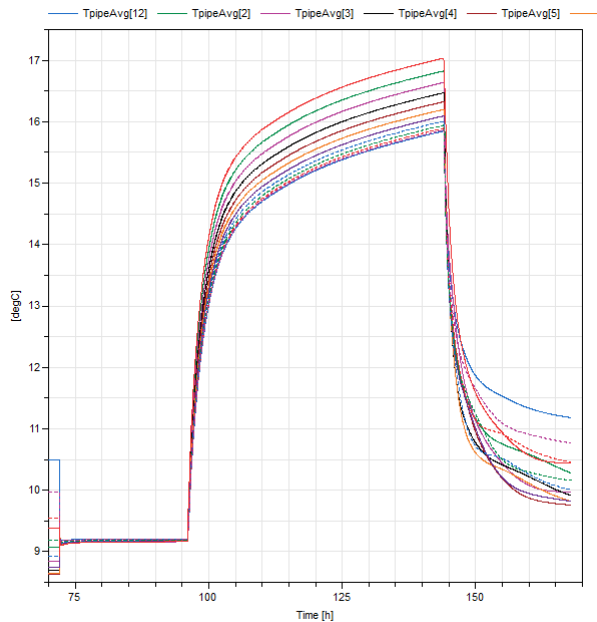


FIG. 22: From Dymola model.

Self-consistency checking

Finally, a self-consistency check of the model was performed. To do this, fluid with a constant temperature of 3 °C was injected into the ground at 0.52 l/s. The ground had the temperature profile of figure 16. Then, the outlet temperature was plotted versus time. In the first test, the size of each Tnode was kept constant, while the extent of the ground (the number of Tnodes) was increased. The eight resulting graphs are compared in figure 23. As

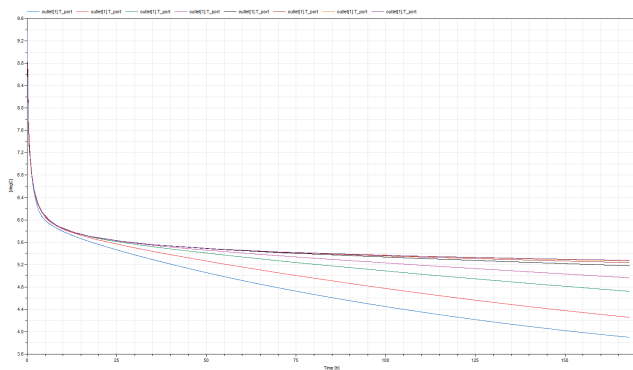


FIG. 23: Comparison of T_{out} for $L_x = L_y = 0.845454$ meters and $n_x = n_y = 6$, $L_x = L_y = 0.986363$ meters and $n_x = n_y = 7$, $L_x = L_y = 1.268181$ meters and $n_x = n_y = 9$, $L_x = L_y = 1.55$ meters and $n_x = n_y = 11$, $L_x = L_y = 2.113636$ meters and $n_x = n_y = 15$, $L_x = L_y = 2.536363$ meters and $n_x = n_y = 18$, $L_x = L_y = 3.10$ meters and $n_x = n_y = 22$ and $L_x = L_y = 3.804545$ meters and $n_x = n_y = 27$.

can be seen, the four graphs corresponding to the finest resolutions are very close together. The end temperature increases with L_x and L_y because the Tnodes are warmer

than the circulating water, and if there are more of them they warm the water more effectively. The 22x22 and the 27x27 graphs are almost overlapping.

Then, a check was done where the resolution for n_x and n_y was increased through 6x6, 11x11, 15x15, 18x18, 22x22 and 27x27, while $L_x = L_y = 3.81$ meters for all resolutions. The result can be seen in figure 24. Again, the graphs are quite close together apart from the graph from the 6x6 resolution (black). As the resolution is increased the difference becomes very small. The end temperature increased with the resolution, which indicates better transfer from the surrounding ground to the circulating water for high resolutions. The spread at the end is about 0.2 °C.

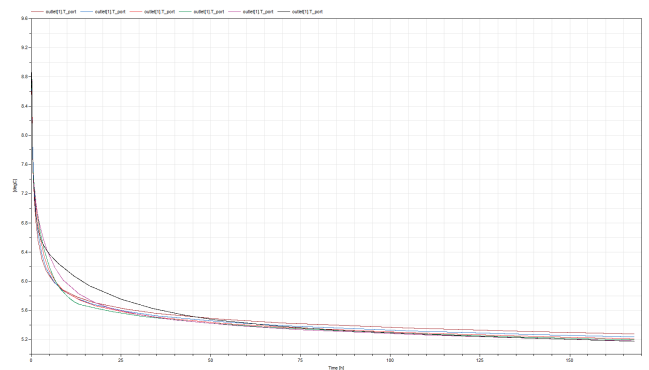


FIG. 24: Comparison of T_{out} for $L_x = L_y = 3.81$ meters and $n_x = n_y = 6, 11, 15, 18, 22$ and 27.

In figure 25, a check was done where $L_x = L_y = 2.1136$ meters, and $n_x, n_y = 5, 7, 9, 11, 13$ and 15. In this case, only odd numbers were chosen because this ensures that the borehole is in the middle of the Tnode array at all times. As before, the end temperature increases with n_x and n_y .

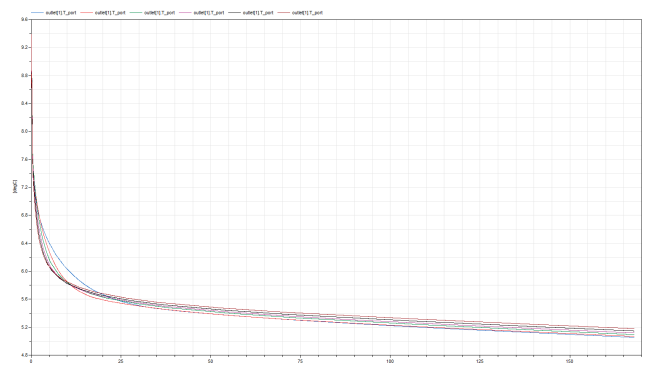


FIG. 25: Comparison of T_{out} for $L_x = L_y = 2.1136$ meters and $n_x = n_y = 5, 7, 9, 11, 13$ and 15.

A check where the size of the ground was increased while keeping $n_x = n_y = 11$ was also done, and the result can be seen in figure 26. The outlet temperature at the end of the simulation seems to slowly converge towards 3

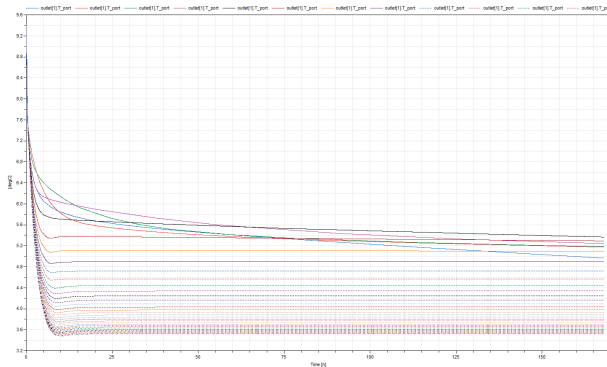


FIG. 26: Comparison of T_{out} for $n_x = n_y = 11$ and $L_x = L_y = 1.55$ meters, 3.10 meters, 6.20 meters, ...etc.

$^{\circ}\text{C}$ as we increase L_x and L_y . This might be because *very* large Tnodes might not respond in time and thus the outlet temperature quickly drops as the inlet water reaches the outlet. When the Tnodes are smaller, they respond quicker and warm up the circulating water, causing the curves to not drop off as rapidly in the beginning.

SIMPLIFIED MODEL FOR COMPUTING

$$T_{out}(T_{in}, T_{ground}(z), \dot{m}, t)$$

The next step was to make a simplified model to represent the boreHole. The model used can be seen in figure 27.

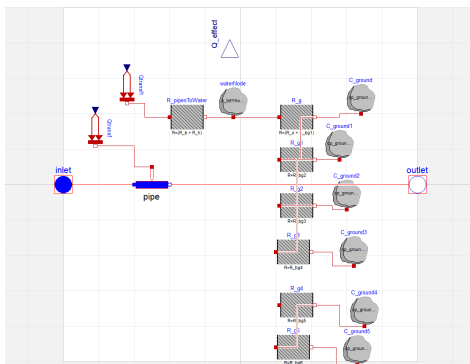


FIG. 27: Simplified model for finding $T_{out}(T_{in}, T_{ground}(z), \dot{m}, t)$.

Here, the pipe element represents pipe0 and pipe1 in the complex model, while the waterNode represents Cb1 and Cb2. The different C_ground elements represents cylindrical shells of soil surrounding the boreHole. The position of each mass node is in the middle of the cylindrical shells. The diameter of the circle intersecting the i th mass node is chosen to be

$$D_{gi} = D_{boreHole} + dFac[i] \cdot distAvailable \quad (34)$$

where $dFac[i]$ is a normalized percentage of the distance between the penetration radius r_{ground} and the

boreHole radius. It thus represents the thickness of a given shell divided by the total thickness of all the shells. $distAvailable$ is the distance between the boreHole radius and r_{ground} .

These diameters are then used in equation (30) to compute R_{bg1} , R_{bg2} etc. However, note that dz needs to be changed in several of the formulas because we now only have one pipe, so dz now represents the entire height of the boreHole times two (because there is two pipes per segment in the complex model). Thus, $dz \rightarrow 2boreHole_{height}$ for R_{bg1} , R_{bg2} etc as well as for R_b and R_x . However, for R_{bb} and R_{pp} $dz \rightarrow boreHole_{height}$ because there is only one of these per segment. The heat capacitance of each such cylindrical shell i is given by

$$C = \rho \cdot c_p \cdot totVolume \cdot dVolFrac[i], \quad (35)$$

where

$$totVolume = \pi \cdot h_{boreHole} \cdot (r_{ground}^2 - 0.25 \cdot D_{boreHole}^2) \quad (36)$$

VolFrac is the volume fraction of a given shell to the total volume of all the shells. A total of 6 groundNodes were chosen, because in the complex model 5 Tnodes were surrounding the boreHole in all 4 directions. This means that we can think of 6 cylindrical shells in the simple model (including the Tnode in which the boreHole is embedded) to represent the complex model.

In the tests that follow, the following is meant by 'heat pulse injection':

- The ground is initialized at 10°C .
- 0.5 l/s at 15°C into the ground for 8 hours.
- Stop injection for four hours.
- Inject 0.5 l/s at 5°C into the ground for 8 hours.
- Stop injection for 21.67 hours.
- Inject 0.5 l/s at 5°C for 18.33 hours.

Comparison of complex and simple model - heat pulse injection

The models agree somewhat, but not perfectly. In this simulation, the penetration radius was set to 1.05 meters in the simple model, while $L_x = L_y = 2.10m$ in the complex model. However, by adjusting the thickness and position of the different cylindrical shells, the result can be made to approach the complex model. The difference between the two models may be due to several reasons. First, the complex model has two pipe-elements instead of one, and two water nodes instead of one. All of these interact with each other. Second, the complex model consists of several boreHole segments, while the simple model only has one, even though this is somewhat compensated

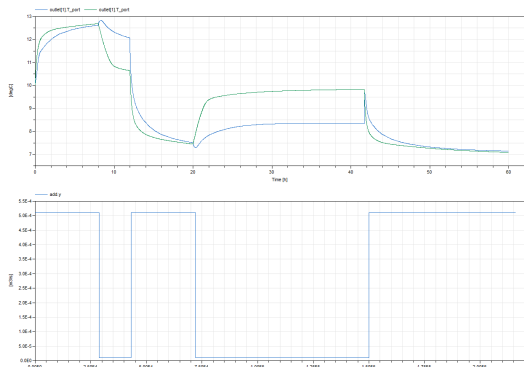


FIG. 28: $T_{out}(T_{in}, T_{ground}(z), \dot{m}, t)$. The blue graph is from the complex model, while the green graph is from the simple model. The lower graph is the volume flow.

for by increasing the thermal masses, reducing the resistances and using LMTD in the simple model. Third, the simple model uses cylindrical shells, which means that any given amount of mass will be closer to the boreHole in the simple model than in the complex model. That is, cylindrical shells is a denser form of packing mass around the boreHole. Thus, in order to make the two models agree, the outermost shell in the simple model needs to be further away than the outermost Tnodes in the complex model. Note that on this third point, the simple model may actually be more correct. It is more natural for heat to move radially as opposed to through a rectangular grid.

Note that during the periods when the fluid pump is switched off there is also a large difference between the two graphs. This is probably due to an LMTD issue in Modelica's pipe element: a linear approximation is used even when the temperature profile inside the pipes is nonlinear, which is the case when the massflow is low. In the simplified model LMTD is used, while in the complex model, Modelica's linear approach is used. By also using a linear approach in the simplified model, the result was as in figure 29.

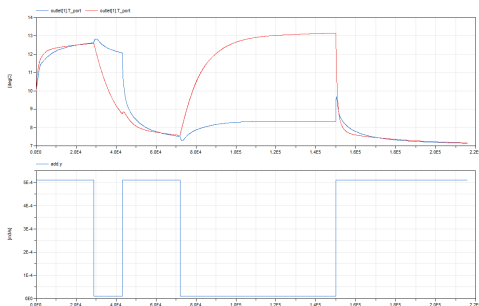


FIG. 29: $T_{out}(T_{in}, T_{ground}(z), \dot{m}, t)$. The blue graph is from the complex model, while the red graph is from the simple model. The lower graph is the volume flow.

As can be seen, the error is even larger here. This means that using LMTD in the simplified model somewhat compensates for the error, but it cannot completely

remove it. Therefore, the LMTD model is used from this point.

Since this error is largest when the massflow is low, and since $Q = \dot{m} \cdot c_p \cdot \Delta T$, this means that the error in Q is small since \dot{m} is small when the error is large. Therefore, Q was also compared for the two simulations. In all models,

$$\Delta T = T_{out} - T_{in}. \quad (37)$$

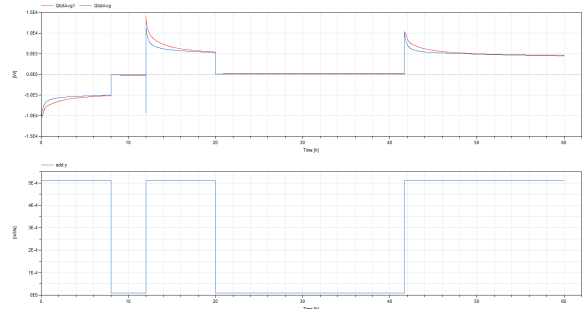


FIG. 30: $Q(T_{ground}(z), \dot{m}, t)$. The red graph is from the complex model, while the blue graph is from the simple model. The lower graph is the volume flow.

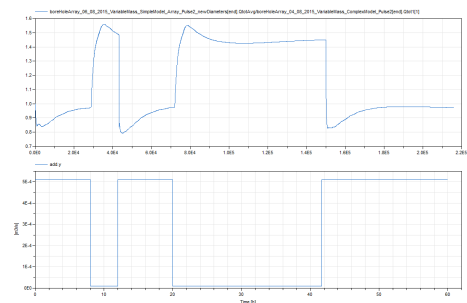


FIG. 31: $\frac{Q_{simple}(T_{ground}(z), \dot{m}, t)}{Q_{complex}(T_{ground}(z), \dot{m}, t)}$.

Figure 30 shows that the two models give quite similar results. Hence, it might be concluded that the error seen in figures 28 and 29 are due to errors in reading off the temperature. In figure 31 it can be seen that the error is within - 20 % as long as the massflow is turned on. When the massflow is turned off, the models do not agree very well. This too is probably caused by some issues with LMTD. It was decided to also use $Q(T_{ground}(z), \dot{m}, t)$ to compare the models from now on.

Sine heat pulse injection

A sine with a period of 24 hours, offset at 10^0 C and amplitude of 5^0 C was injected into a ground which had a temperature of 10^0 C. The massflow was constant and

equal to 0.5 l/s at all times. The result can be seen in figures 32 and 33.

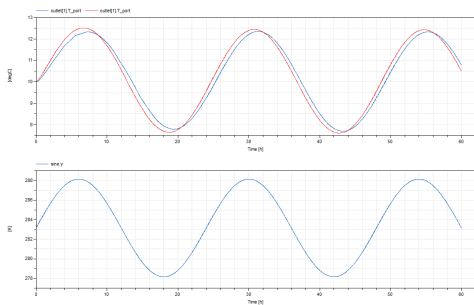


FIG. 32: $T_{out}(T_{in}, T_{ground}(z), \dot{m}, t)$. The blue graph is from the complex model, while the red graph is from the simple model. The lower graph is T_{in} .

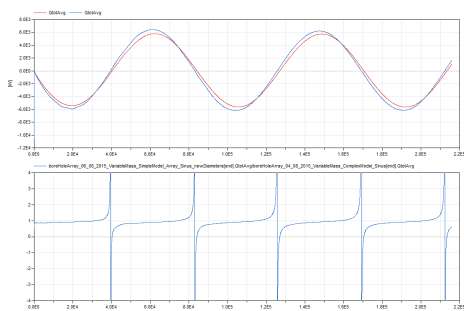


FIG. 33: $Q(T_{in}, T_{ground}(z), \dot{m}, t)$. The blue graph is from the complex model, while the red graph is from the simple model. The lower graph is $\frac{Q_{simple}(T_{ground}(z), \dot{m}, t)}{Q_{complex}(T_{ground}(z), \dot{m}, t)}$.

BoreHole B2G model with cylindrical shells

A model, boreHole_withCapacitances_OnlyOne, was made for only one boreHole where the groundSegment model is dropped as it is only necessary for modelling several boreHoles. This model had the boreHole heat-Port array connected in series to several arrays of cylindrical concentric disks surrounding the boreHole. The position of the soil nodes, the extent of the cylindrical shells, their capacitance and geometry etc. is calculated in the same way as for the simplified model. The purpose of the model is to investigate how much difference between a rectangular grid and cylinder shells matters. That is, when we compare the complex model to the simple, the complex model has the boreHole embedded in a rectangular grid, while the simple model has concentric mass rings around the boreHole. This means that there is a difference in the way the heat flux moves in the two models. In order to see how large this effect is, a model where the same boreHole model is used, but with concentric shells instead was constructed. The outlet temperature was then compared to the outlet temperature from the complex model. A comparison was also done for Q. See

next section.

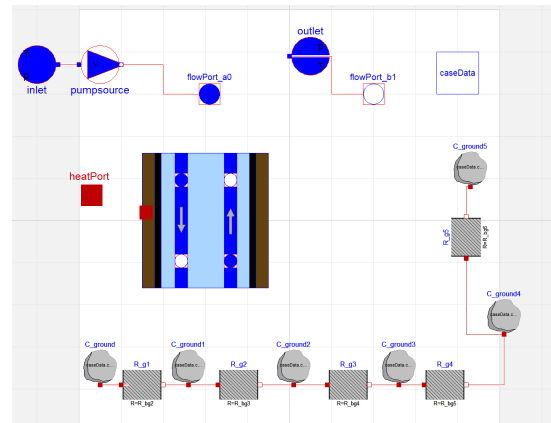


FIG. 34: Overview of the boreHole B2G model with cylindrical shells for one hole, based on the boreHoleSegment model.

Comparison of the complex model and B2G model with cylindrical shells - heat pulse injection

A comparison was done between the complex model with $L_x = L_y = 2.1m$ and the B2G model with cylindrical shells and $r_{ground} = 1.05$.

The result can be seen in figures 35 and 36. As can be seen in the upper plot, the models agree fairly well. Also note that the error between the two models in $T(T_{in}, T_{ground}(z), \dot{m}, t)$ is small even when the mass flow is off. This means that some internal difference in the model creates the large error in $T(T_{in}, T_{ground}(z), \dot{m}, t)$ between the simple model and the complex model when the volume flow is off. Otherwise, the two models compared here, which are equal internally, would have had an equally large error when the volumeflow is off. As can be seen, the ratio never exceeds 1.30 in figure 36.

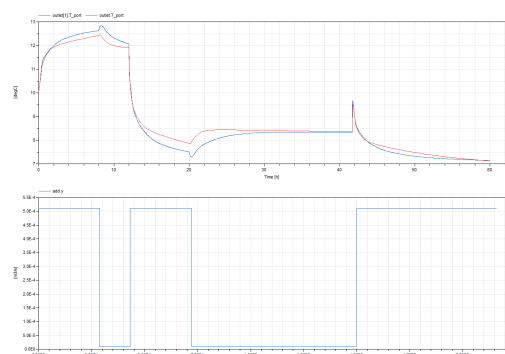


FIG. 35: Comparison of $T_{out}(T_{in}, T_{ground}(z), \dot{m}, t)$ from the boreHole B2G with cylindrical shells model (red graph) and from the complex model (blue graph). The lower graph is the volume flow.

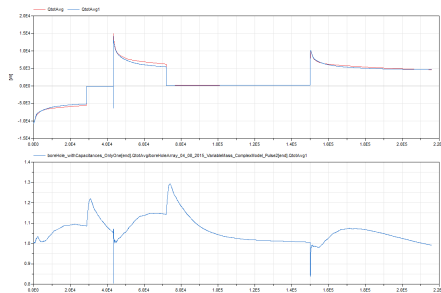


FIG. 36: Comparison of $Q(T_{in}, T_{ground}(z), \dot{m}, t)$ from the boreHole B2G with cylindrical shells model (red graph) and from the complex model (blue graph). The lower graph is $\frac{Q_{cylinder-shell}(T_{ground}(z), \dot{m}, t)}{Q_{complex}(T_{ground}(z), \dot{m}, t)}$.

Comparison of the complex model with one boreHole versus the simplified model and the B2G model with cylindrical shells - heat pulse injection

In figure 37, the result for $T_{out}(T_{in}, T_{ground}(z), \dot{m}, t)$ from the simplified model was added to figure 35.

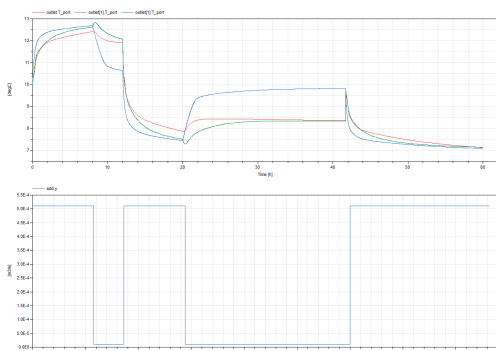


FIG. 37: Comparison of $T(T_{in}, T_{ground}(z), \dot{m}, t)$ from the boreHole B2G with cylindrical shells model and from the simplified model as well as from the complex model. The blue graph is the simplified model, the red is the B2G with cylinder shells and the green is the complex model. The lower graph is the volume flow.

As can be seen in figure 37, the simplified model, which uses LMTD internally, has a different response when the water is turned off. Therefore, this graph is not very useful due to problems with reading off the temperature. However, this problem is avoided by adding the result for $Q(T_{in}, T_{ground}(z), \dot{m}, t)$ from the simplified model to figure 36 instead, as can be seen in figure 38.

From figure figure 38, it seems like the B2G with cylindrical shells model is slightly more similar to the complex model than the simplified model is. The exact reason for this is unknown, but it is probably because the two former models share the same internal configuration: the boreHoleSegments.

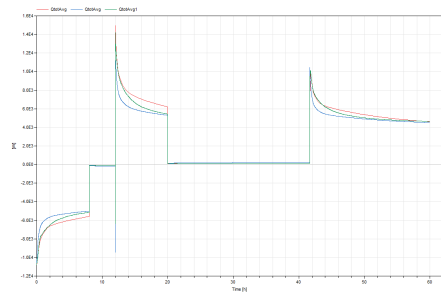


FIG. 38: Comparison of $Q(T_{in}, T_{ground}(z), \dot{m}, t)$ from the boreHole B2G with cylindrical shells model and from the simplified model as well as from the complex model. The blue graph is the simplified model, the red is the B2G with cylinder shells and the green is the complex model.

Comparison of a complex boreHole with only one node in the z-direction, versus the same model with $nz = 6$ and $nzWell = 5$ - heat pulse injection

This test was done to see whether the resolution in the z-direction is of any importance. The simplified model consists of only one very long pipe element, and this might give rise to some errors. Hence, this graph will tell us how much of the error is due to a lack of resolution in the z-direction. If this is indeed the case, one might consider connecting the simple model in series to increase the z-resolution.

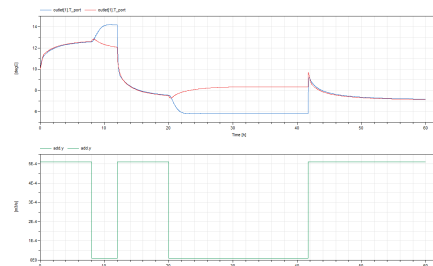


FIG. 39: Comparison of the complex boreHole model outlet temperature $T_{out}(T_{in}, T_{ground}(z), \dot{m}, t)$ for $nz = nzWell = 1$ (blue graph) and for $nzWell = 5, nz = 6$ (red graph). Note that in both cases, the actual depth of the boreHole is 260 meters.

The result can be seen in figures 39 and 40, and it is seen that the resolution in the z-direction is of little importance.

Comparison of arrays of boreHoles and a single boreHole - heat pulse injection

First, a test was done with a 2x3 array of boreHoles with a groundSegment of 2.25 m times 2.75 meters. A small groundSegment was first chosen to clearly see the interaction between the boreHoles. One would expect that the boreHoles should split into two categories: corners (4 of them) and sides (two of them). This is indeed

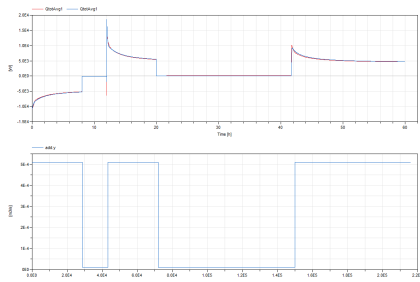


FIG. 40: Comparison of the complex boreHole model effect $Q(T_{in}, T_{ground}(z), \dot{m}, t)$ for $nzWell = 1$ (blue graph) and for $nzWell = 5, nz = 6$ (red graph). Note that in both cases, the actual depth of the boreHole is 260 meters.

the case, as can be seen in figure 41.

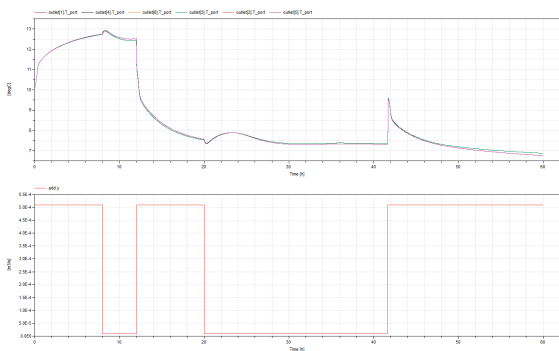


FIG. 41: Comparison of all the boreHole outlets $T_{out}(T_{in}, T_{ground}(z), \dot{m}, t)$ in a 2x3 array. As can be seen, the six boreHoles split into two groups: corners and sides.

Then, a series of test with the following parameters was done:

- Single boreHole: $n_x = n_y = 7, L_x = L_y = 17.5m$.
- 2x3 boreHole: $n_x = 9, n_y = 11, L_x = 22.5m, L_y = 27.5m, nxGap = nyGap = 1$.
- 3x4 boreHole: $n_x = 11, n_y = 13, L_x = 27.5m, L_y = 32.5m, nxGap = nyGap = 1$.
- 4x5 boreHole: $n_x = 13, n_y = 15, L_x = 32.5m, L_y = 37.5m, nxGap = nyGap = 1$.

These parameters were chosen carefully to keep the same distance from the boreHoles to the edges (8.75 meters) and the same distance between the boreHoles (5 meters) in all directions.

Figure 42 demonstrates that the interaction between the boreHoles in the arrays matters because the graph of the single boreHole deviates from the other graphs. However, this deviation is only present when the volume flow is turned off.

In figure 43 the effect per borehole is plotted for a single borehole and also for the average in a 2x3 array, a 3x4 array as well as a 4x5 array. As can be seen from

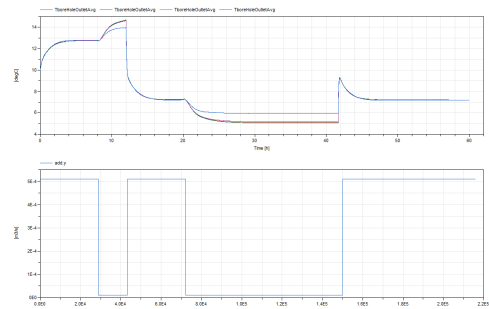


FIG. 42: Comparison of $T_{out}(T_{in}, T_{ground}(z), \dot{m}, t)$ for one single boreHole versus 2x3, 3x4 and 4x5 arrays of boreHoles. The single boreHole is represented by the blue graph, and deviates slightly from the rest. The rest of the arrays seem to have fairly similar responses. The lower graph is the volume flow.

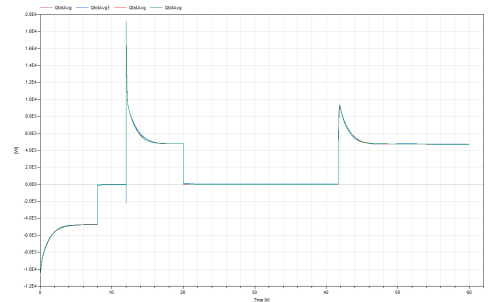


FIG. 43: Comparison of Q per boreHole in a single boreHole versus in a 2x3 array, a 3x4 array and a 4x5 array of boreHoles. At all times, the distance between the boreHoles is 5 meters.

figure 43, the response is fairly similar for the different configurations if the separation is at least 5 meters. The error seen in figure 42 is negligible because it was mostly present when \dot{m} was small.

Simplified model approximating array of boreHoles

The next step would be to implement a simplified model approximating the complex array model. This could be done by making a separate simulation for each boreHole in the ground. That is, given e.g. a 2x3 array of boreHoles, form factors could be used to compute the sum of the heat fluxes from the other boreHoles. Then we add $Q_{Other-boreHoles}(\phi)$ to the simplified model. This must be done for the corner group and the side group in the above example. Hence, two models are needed in that case. For more complex groupings, several simplified models are needed as there are more groups. However, this would be a steady-state model, and might not be a good solution for dynamic short-term simulations. Another option is to keep the current simplified model as a sufficient approximation. It could be improved by customizing it to give similar results as a given configuration of boreHoles, e. g. a 2x3 rectangle. If the configuration is

changed, the parameters in the simple model would have to be adjusted. This might be the most simple solution to implement.

Conclusion

The model developed here gives a good approximation for the response of a BHE to a distributed thermal response test (DTRT). The model can be used to set up any rectangular grid of boreHoles and simulate their behaviour and interaction with each other. The simplified model made to approximate this model seems to give fairly similar responses to the complex model, but it is not good when the volume flow is low. Furthermore, it seems like the average effect of a boreHole in an array is quite similar to that of a single boreHole based on figure 43. Hence, the simplified model could work as an approximation to a boreHole in an array of boreHoles during a DTRT, if the boreHoles keep at least 5 meters distance. In each case, a custom adjustment of the parameters in the simple model should be done. This last point is especially important for long-term simulations where the interactions between the boreHoles likely are more important.

* Electronic address: theodoho@stud.ntnu.no

- [1] F. Ruiz-Calvo, M. De Rosa, J. Acuna, J. Corberan, and C. Montagud, "Experimental validation of a short-term borehole-to-ground (b2g) dynamic model," *Applied Energy*, vol. 140, pp. 210–223, 2015.
- [2] F. Ruiz-Calvo, M. De Rosa, J. Acuna, J. Corberan, C. Montagud, and L. Tagliafico, "Borehole modelling: a comparison between a steady-state model and a novel dynamic model in a real on/off gshp operation," *Journal of Physics: Conference Series*, vol. 547, 2014.
- [3] V. Partenay, P. Riederer, T. Salque, and E. Wurtz, "The influence of the borehole short-time response on ground source heat pump system efficiency," *Energy and buildings*, vol. 43, pp. 1280–1287, 2011.
- [4] J. Acuna, P. Morgensen, and B. Palm, "Distributed thermal response test on a u-pipe borehole heat exchanger," *Effstock - the 11th international conference on energy storage, Stockholm*, 2009.
- [5] P. Stephan, S. Kabelac, M. Kind, H. Marin, D. Mewes, and K. Schaber, *VDI Heat Atlas*. 2 ed., 2010.
- [6] J. Acuna, "Distributed thermal response test - new insights on u-pipe and coaxial heat exchangers in groundwater-filled boreholes. phd thesis, kth.," 2013.
- [7] C. Mallet, "Numerical analysis of a distributed thermal response test on a u-pipe borehole heat exchanger," *Master of Science Thesis, KTH Industrial Engineering and Management*, 2013.
- [8] O. Stavset, "State of the art - Ground source Heat Pumps," *Sintef-notat*, 2013.
- [9] S. Javed and P. Fahlen, "Thermal response testing of a multiple borehole ground heat exchanger," *International Journal of Low-Carbon Technologies*, 2010.
- [10] T. H. Leibel, "Influence of groundwater on measurements of thermal properties in fractured aquifers," *Thesis for the degree of Philosophiae Doctor, Norwegian University of Science and Technology, Faculty of Engineering Science and Technology. Department of Geology and Mineral Resources*, 2012.
- [11] A. Melinder, "Thermophysical properties of aqueous solutions used as secondary working fluids," *Doctoral Thesis, Division of Applied Thermodynamics and Refrigeration, Dept. of Energy Technology*, 2007.

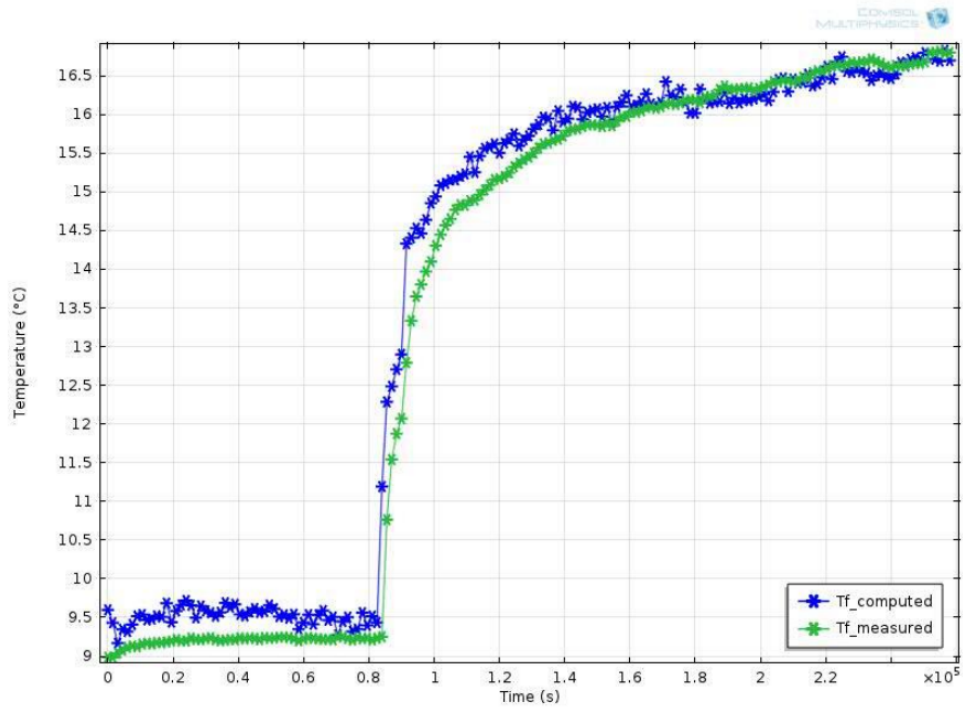


Figure 28: Measured and computed temperatures of the circulating fluid after optimization of R_b for Section 1.

FIG. 44: Average temperature of the two pipe segments in segment 1 as a function of simulation time in [7].

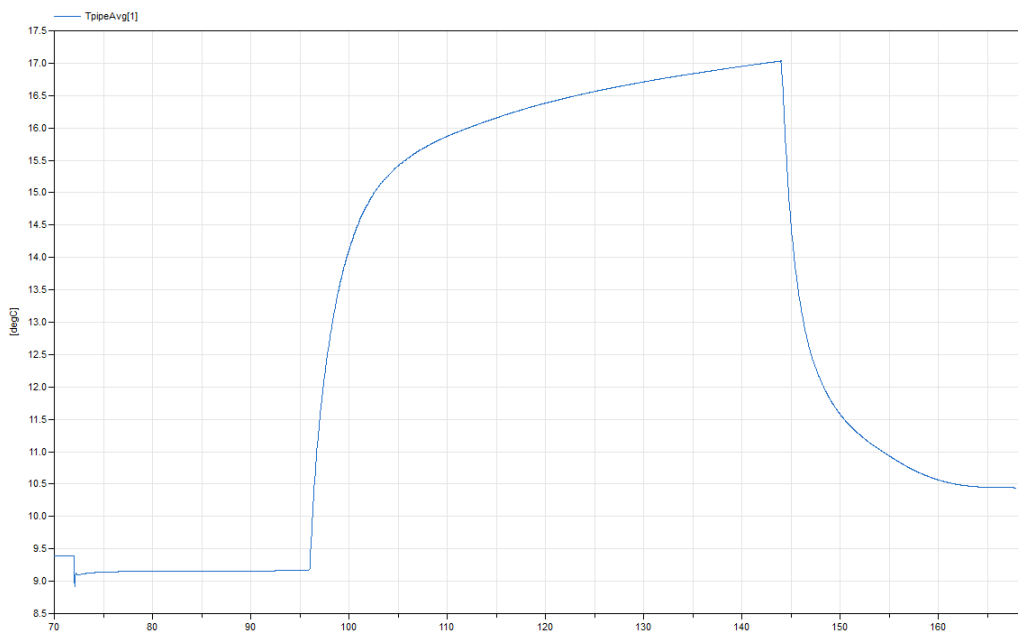


FIG. 45: Average temperature of the two pipe segments in segment 1 as a function of simulation time in Dymola.

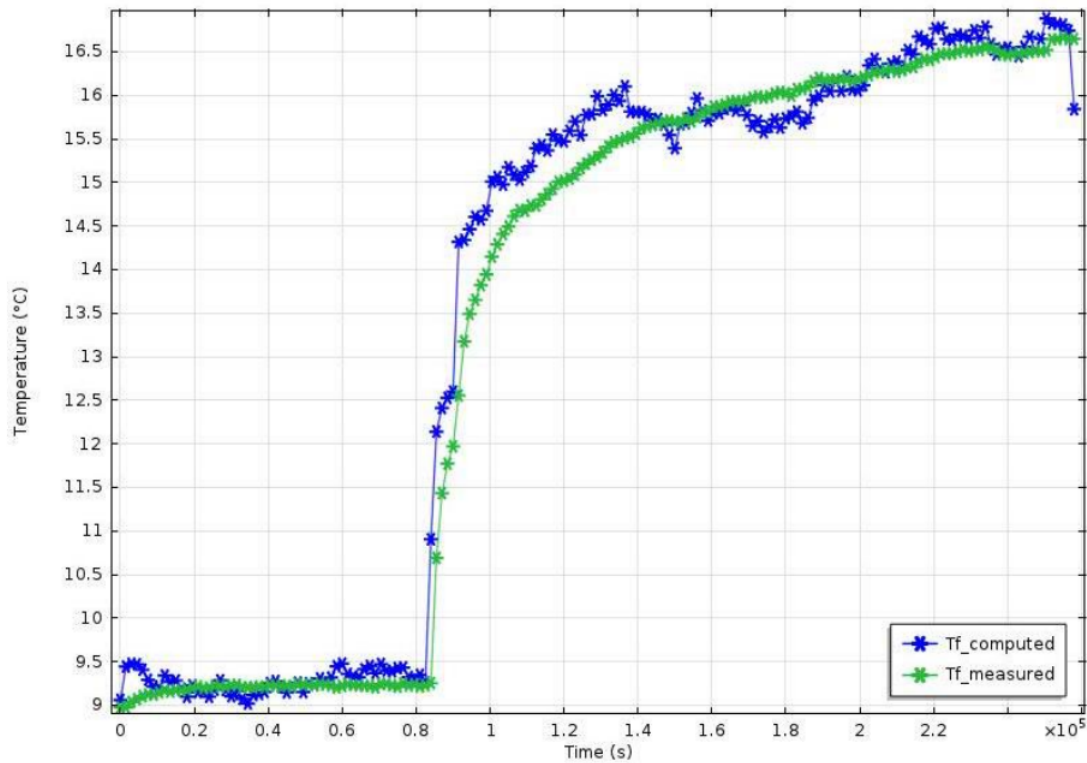


Figure 29: Measured and computed temperatures of the circulating fluid after optimization of R_b for Section 2.

FIG. 46: Average temperature of the two pipe segments in segment 2 as a function of simulation time in [7].

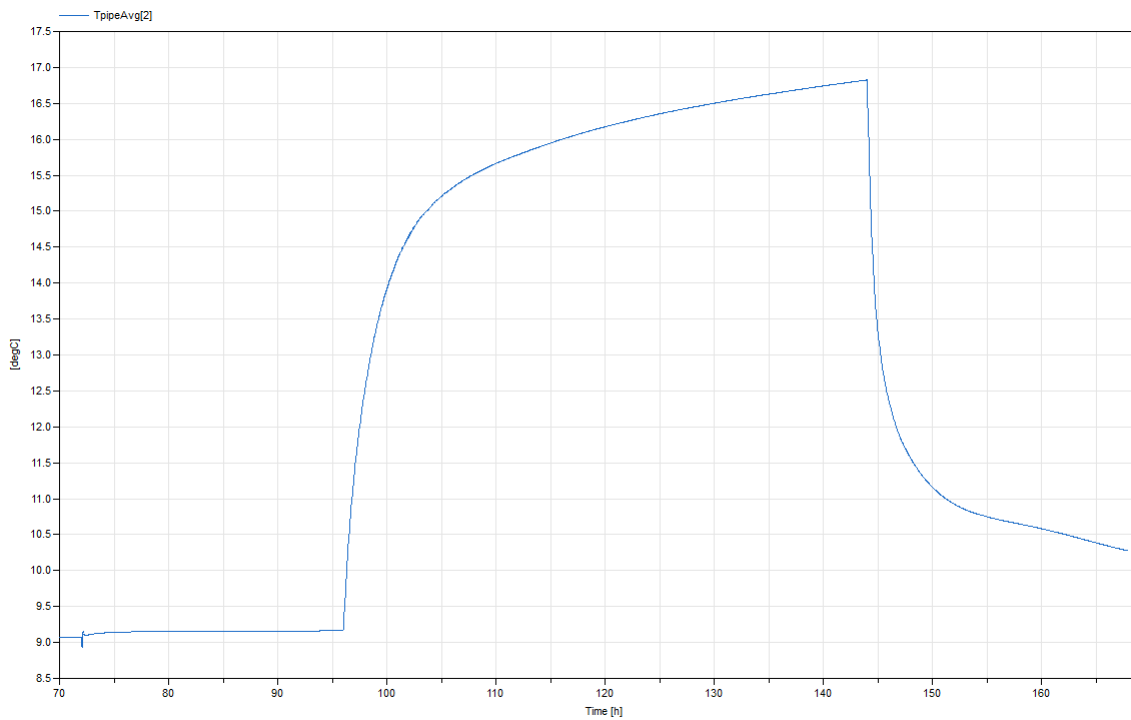


FIG. 47: Average temperature of the two pipe segments in segment 2 as a function of simulation time in Dymola.

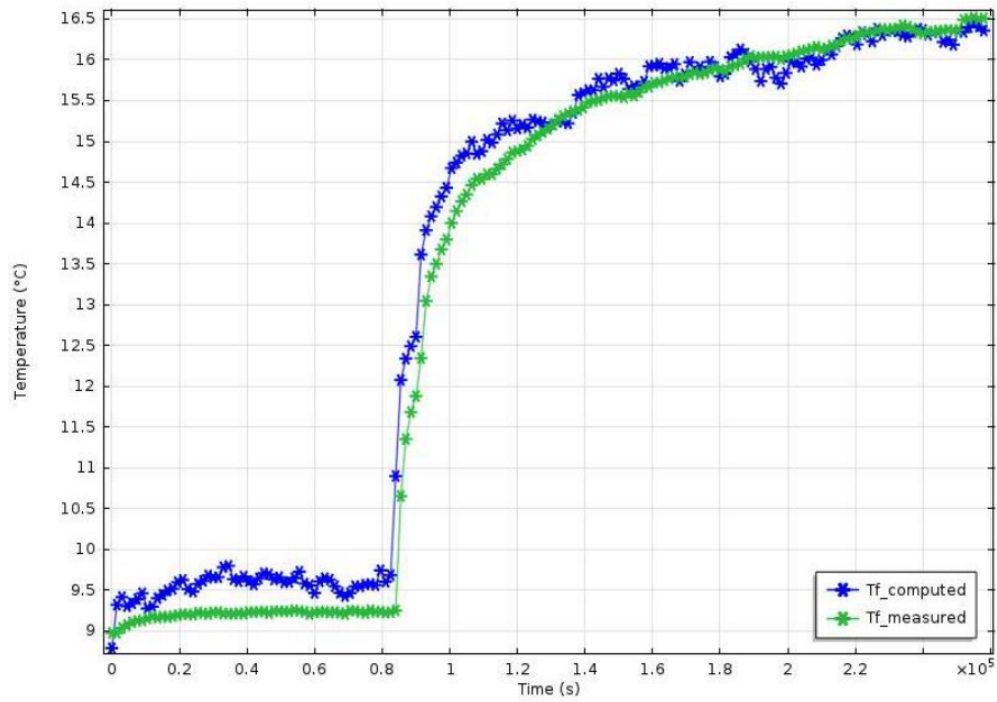


Figure 30: Measured and computed temperatures of the circulating fluid after optimization of Rb for Section 3.

FIG. 48: Average temperature of the two pipe segments in segment 3 as a function of simulation time in [7].

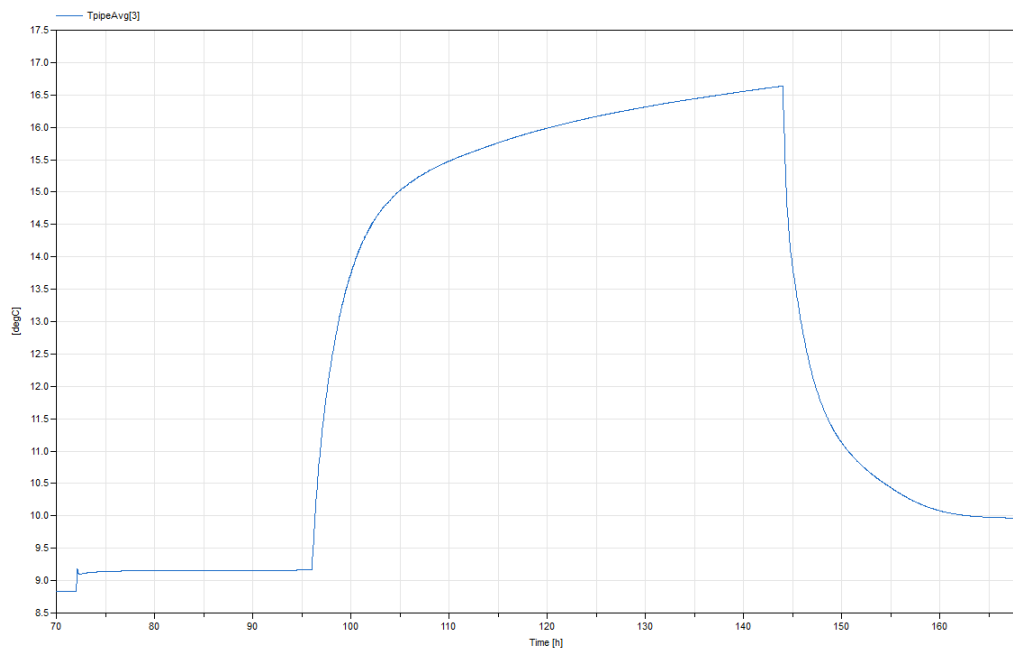


FIG. 49: Average temperature of the two pipe segments in segment 3 as a function of simulation time in Dymola.

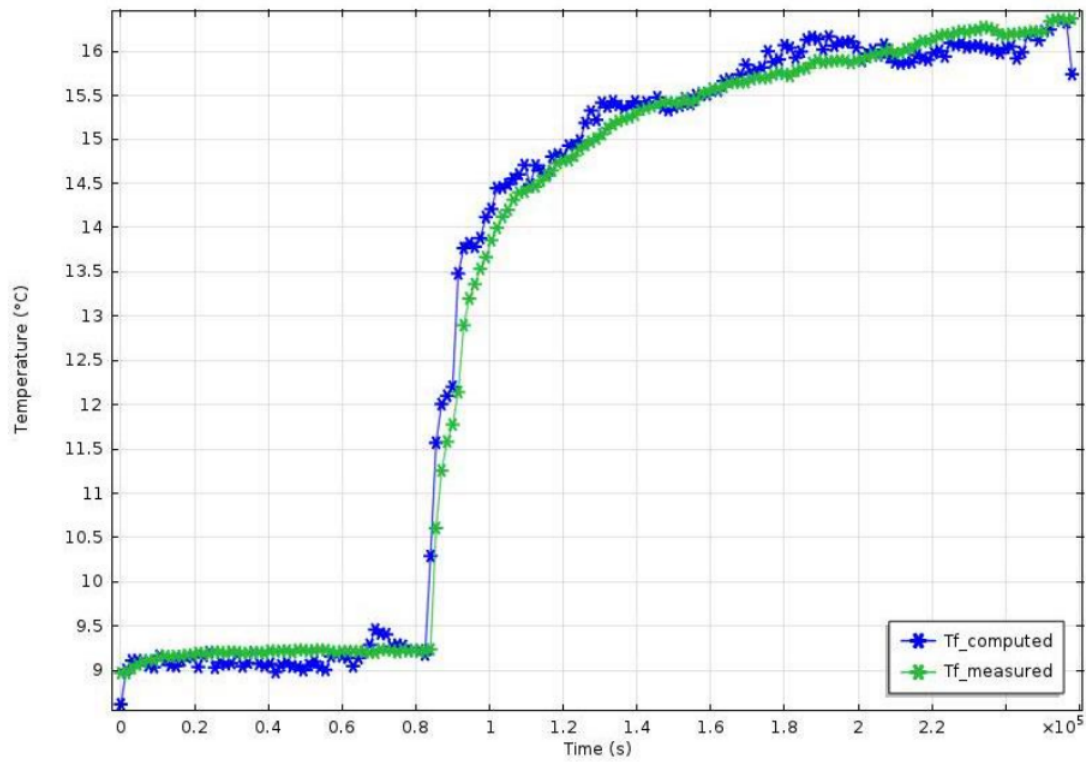


Figure 31: Measured and computed temperatures of the circulating fluid after optimization of R_b for Section 4.

FIG. 50: Average temperature of the two pipe segments in segment 4 as a function of simulation time in [7].

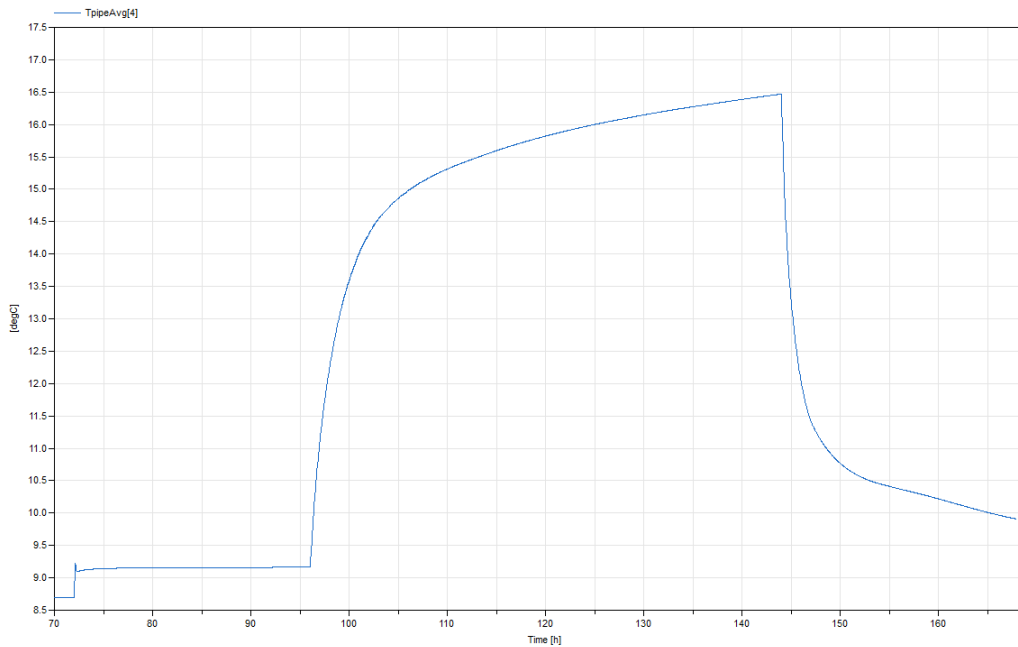


FIG. 51: Average temperature of the two pipe segments in segment 4 as a function of simulation time in Dymola.

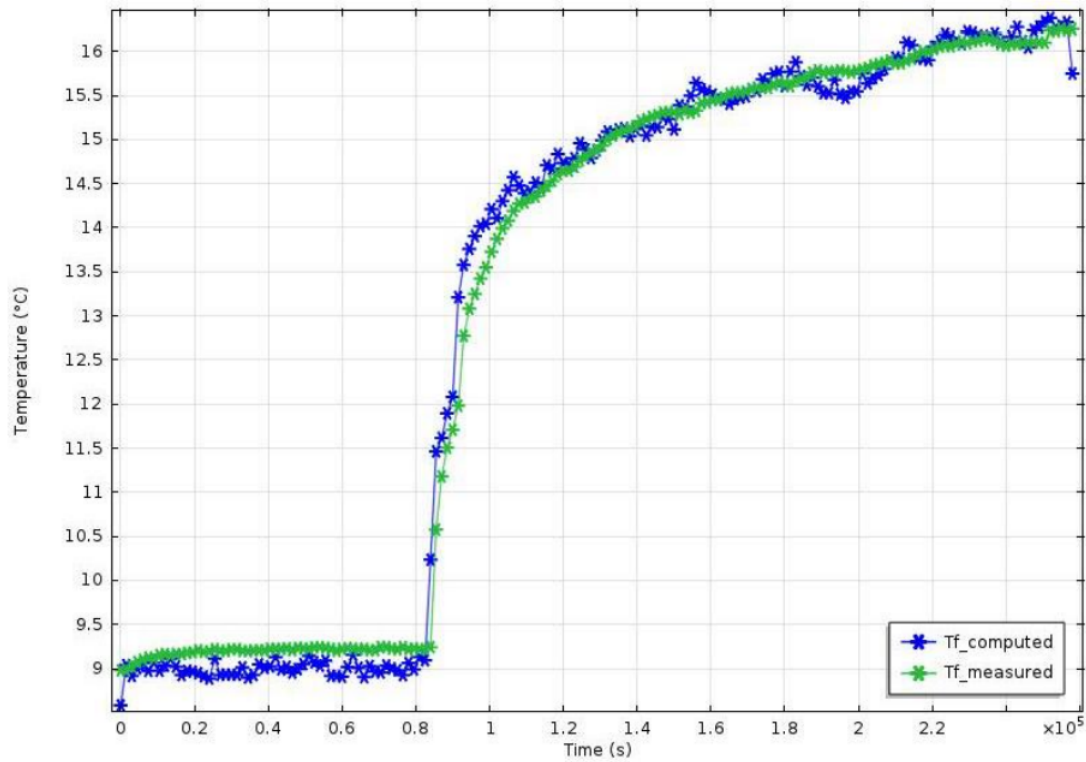


Figure 32: Measured and computed temperatures of the circulating fluid after optimization of R_b for Section 5.

FIG. 52: Average temperature of the two pipe segments in segment 5 as a function of simulation time in [7].

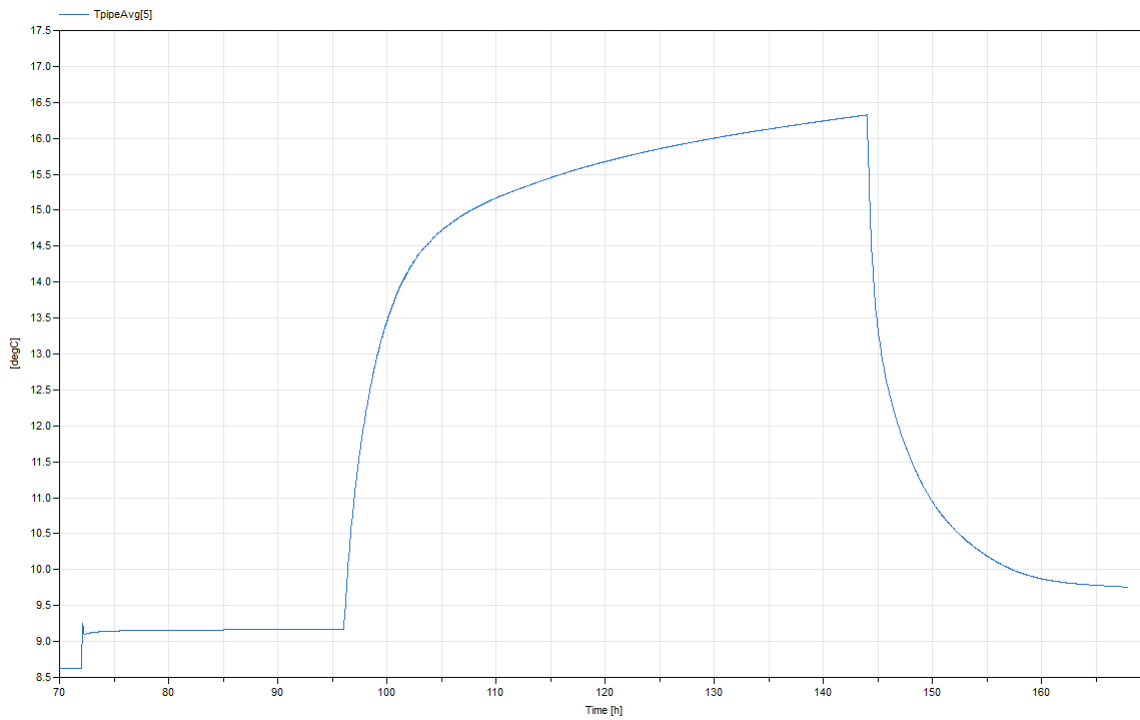


FIG. 53: Average temperature of the two pipe segments in segment 5 as a function of simulation time in Dymola.

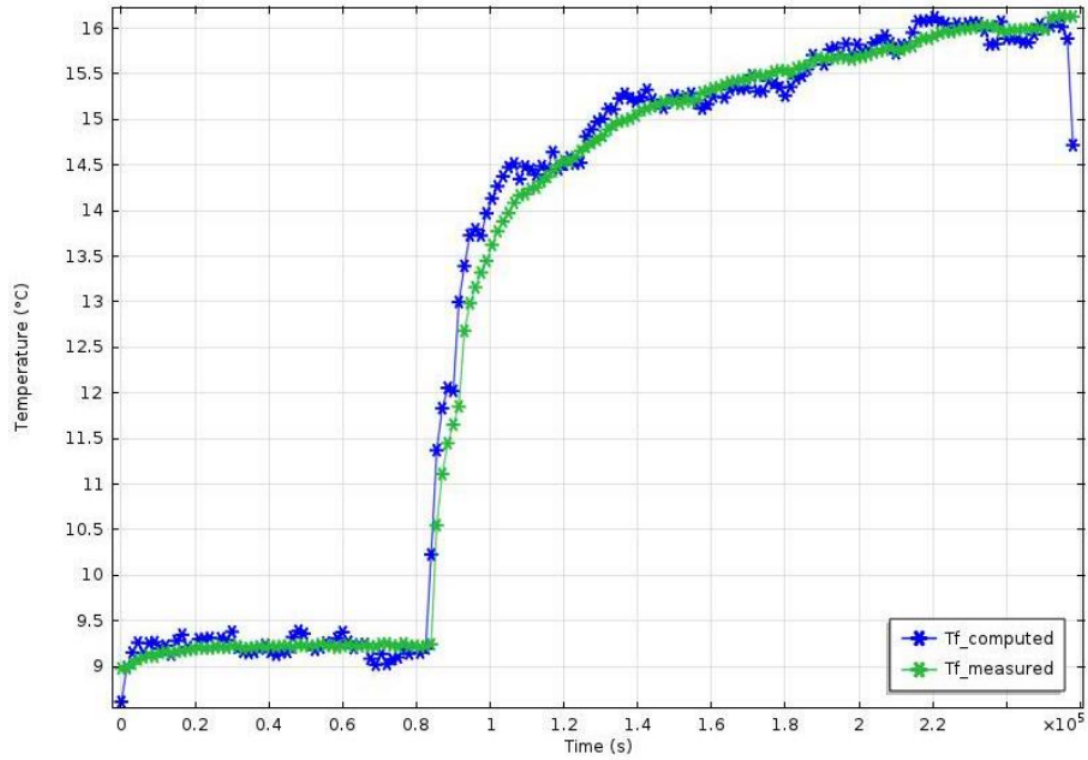


Figure 33: Measured and computed temperatures of the circulating fluid after optimization of R_b for Section 6.

FIG. 54: Average temperature of the two pipe segments in segment 6 as a function of simulation time in [7].

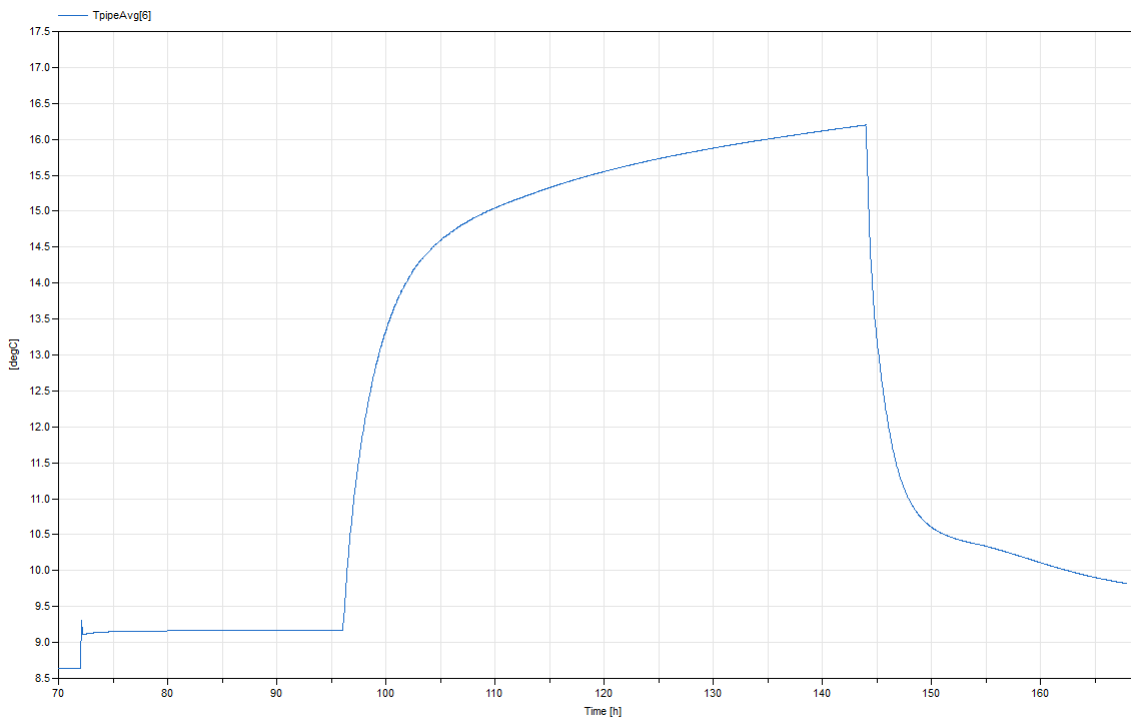


FIG. 55: Average temperature of the two pipe segments in segment 6 as a function of simulation time in Dymola.

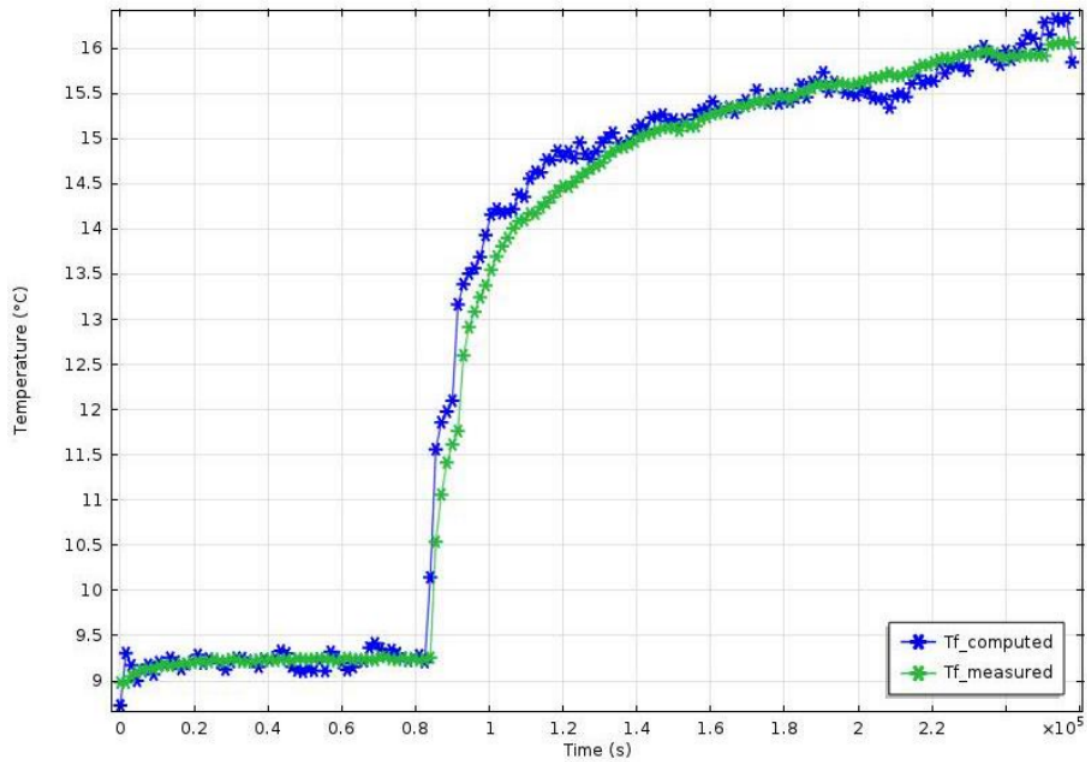


Figure 34: Measured and computed temperatures of the circulating fluid after optimization of R_b for Section 7.

FIG. 56: Average temperature of the two pipe segments in segment 7 as a function of simulation time in [7].

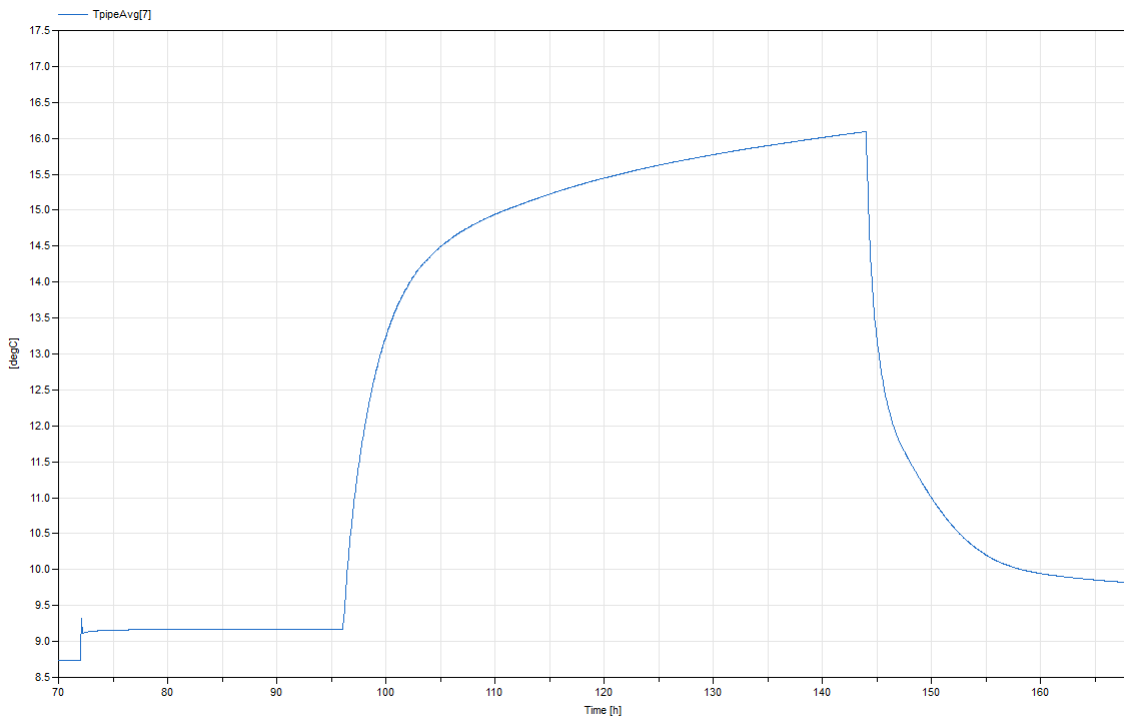


FIG. 57: Average temperature of the two pipe segments in segment 7 as a function of simulation time in Dymola.

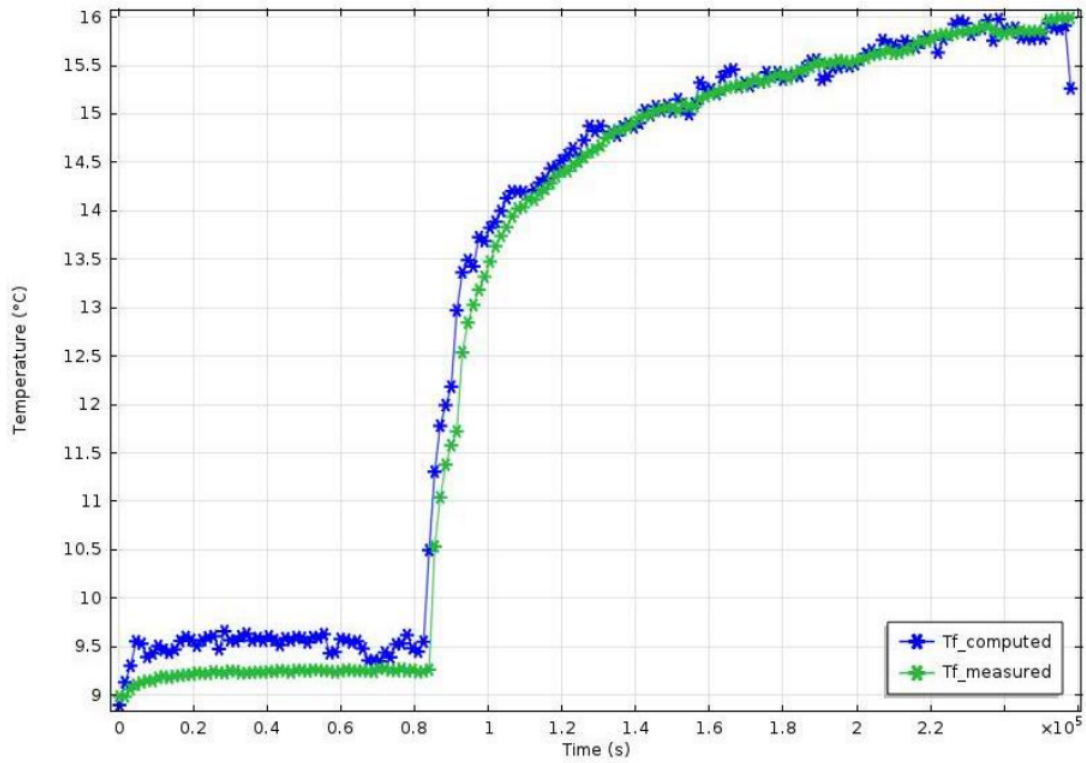


Figure 35: Measured and computed temperatures of the circulating fluid after optimization of Rb for Section 8.

FIG. 58: Average temperature of the two pipe segments in segment 8 as a function of simulation time in [7].

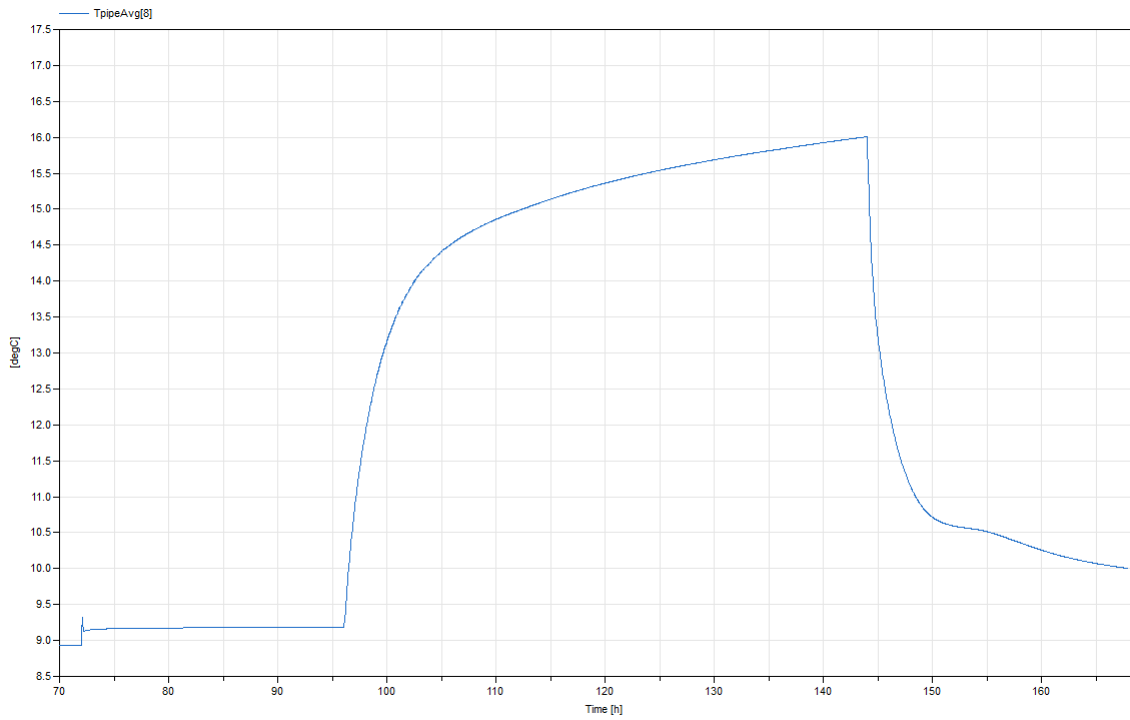


FIG. 59: Average temperature of the two pipe segments in segment 8 as a function of simulation time in Dymola.

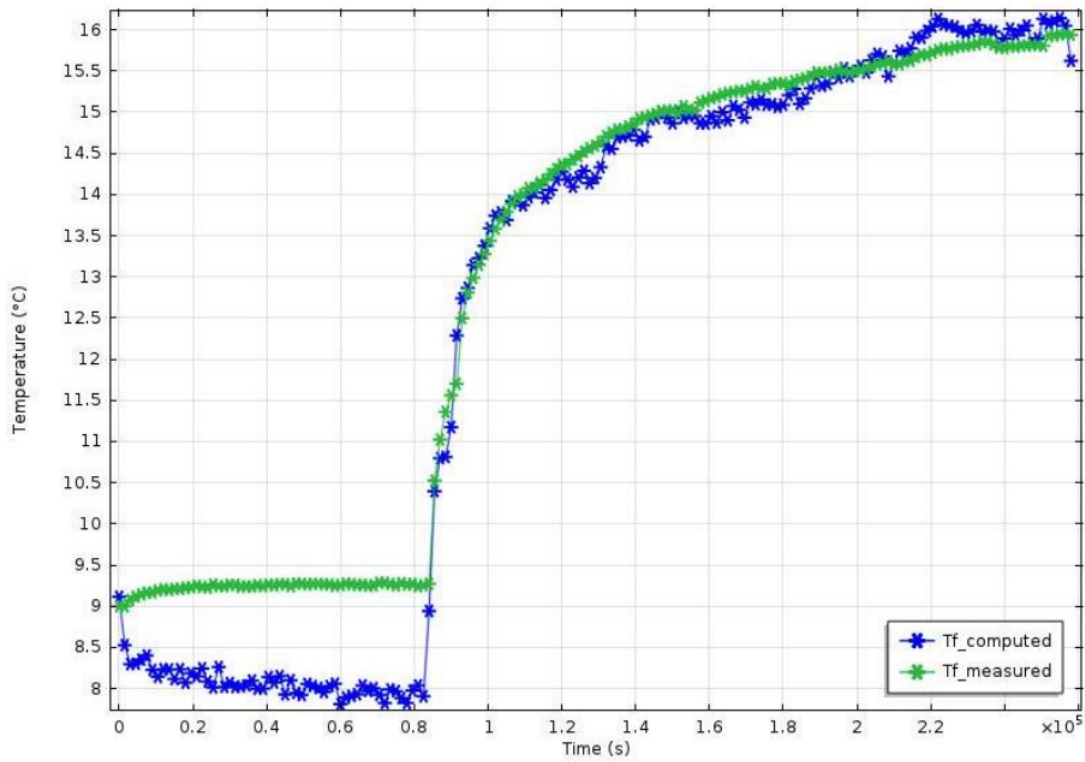


Figure 36: Measured and computed temperatures of the circulating fluid after optimization of R_b for Section 9.

FIG. 60: Average temperature of the two pipe segments in segment 9 as a function of simulation time in [7].

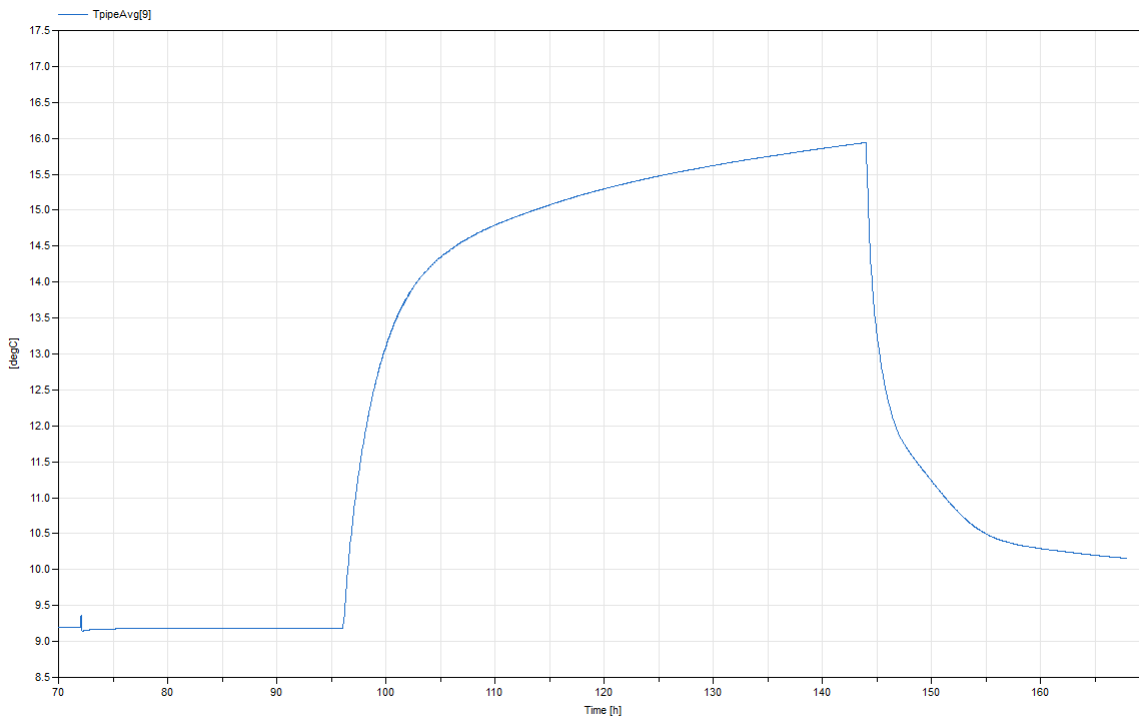


FIG. 61: Average temperature of the two pipe segments in segment 9 as a function of simulation time in Dymola.

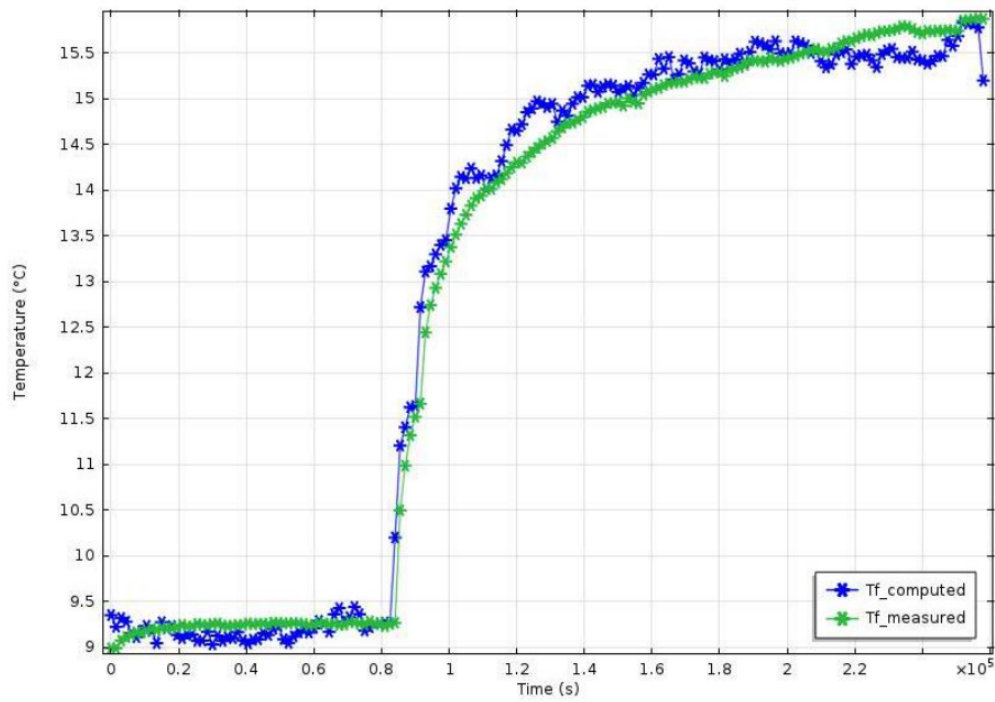


Figure 37: Measured and computed temperatures of the circulating fluid after optimization of R_b for Section 10.

FIG. 62: Average temperature of the two pipe segments in segment 10 as a function of simulation time in [7].

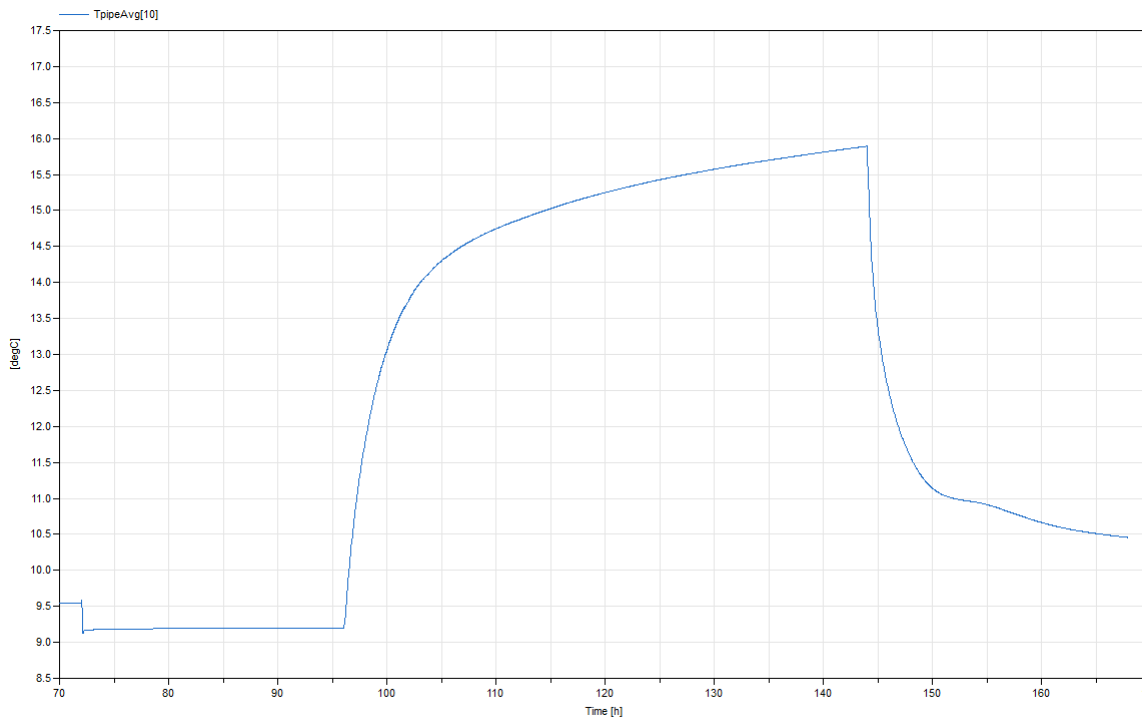


FIG. 63: Average temperature of the two pipe segments in segment 10 as a function of simulation time in Dymola.

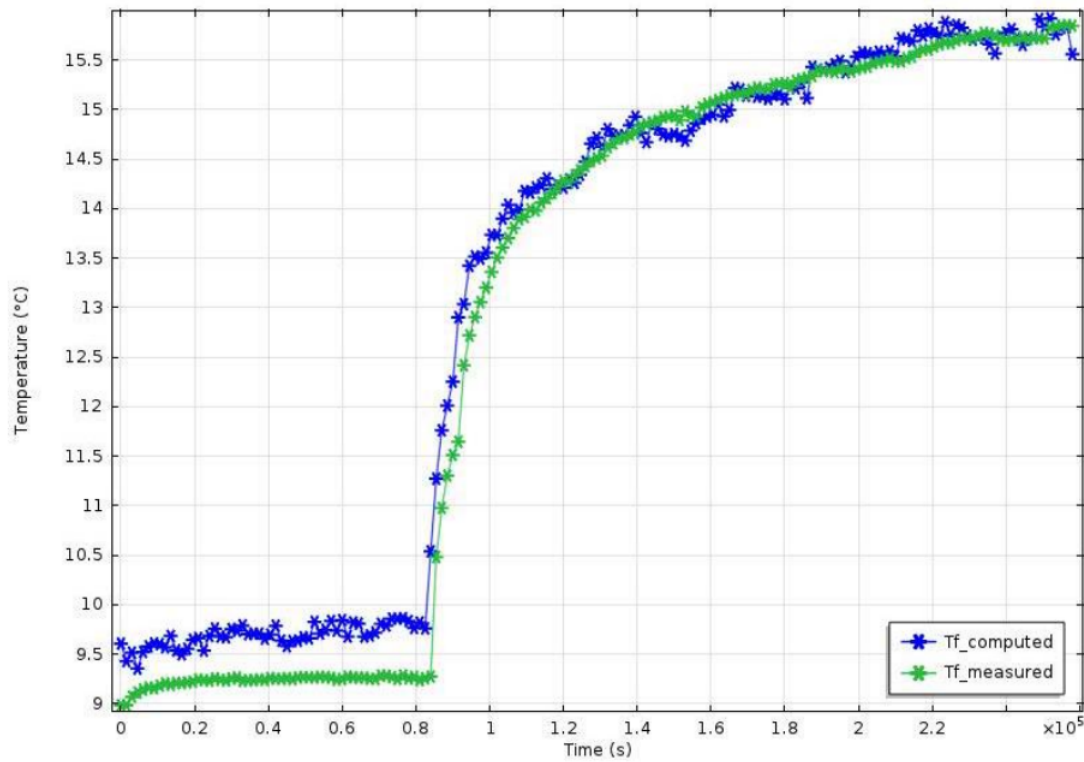


Figure 38: Measured and computed temperatures of the circulating fluid after optimization of R_b for Section 11.

FIG. 64: Average temperature of the two pipe segments in segment 11 as a function of simulation time in [7].

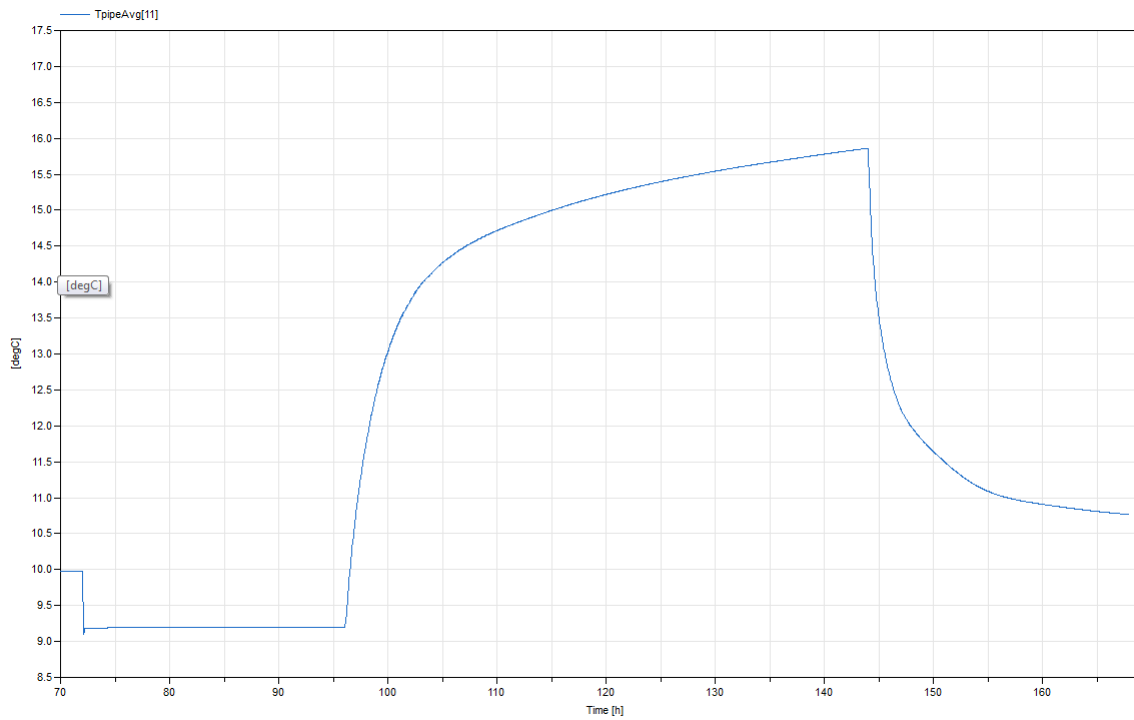


FIG. 65: Average temperature of the two pipe segments in segment 11 as a function of simulation time in Dymola.

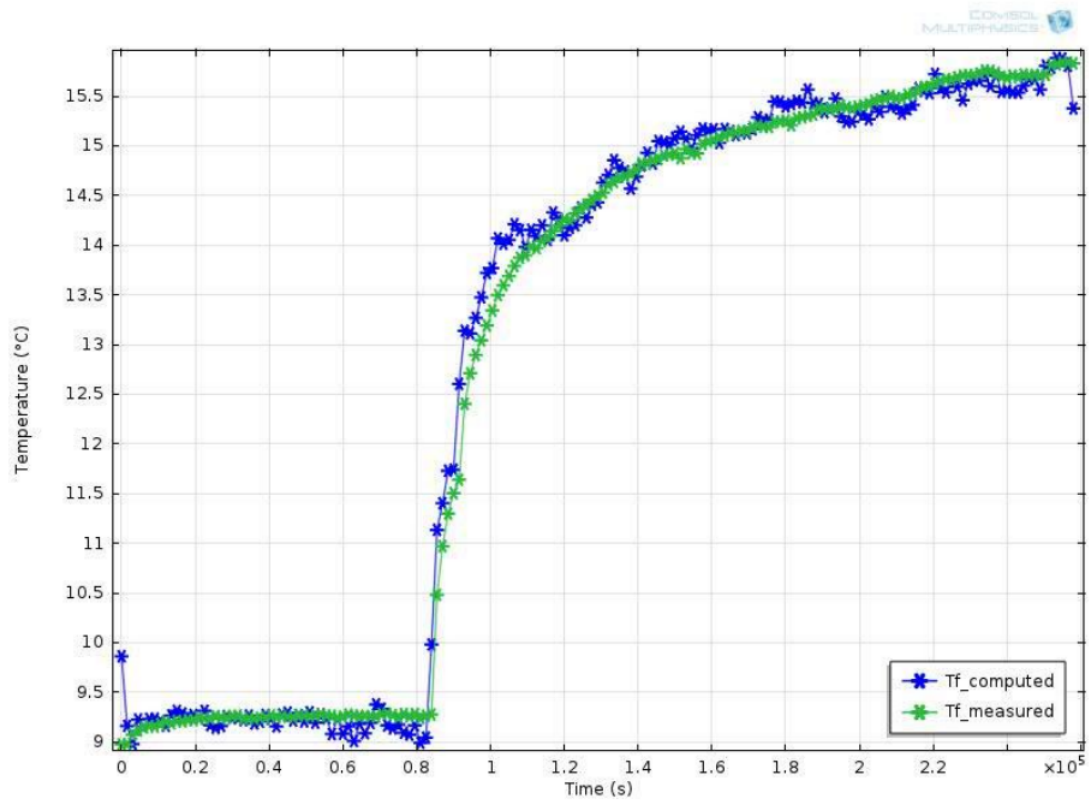


Figure 39: Measured and computed temperatures of the circulating fluid after optimization of R_b for Section 12.

FIG. 66: Average temperature of the two pipe segments in segment 12 as a function of simulation time in [7].

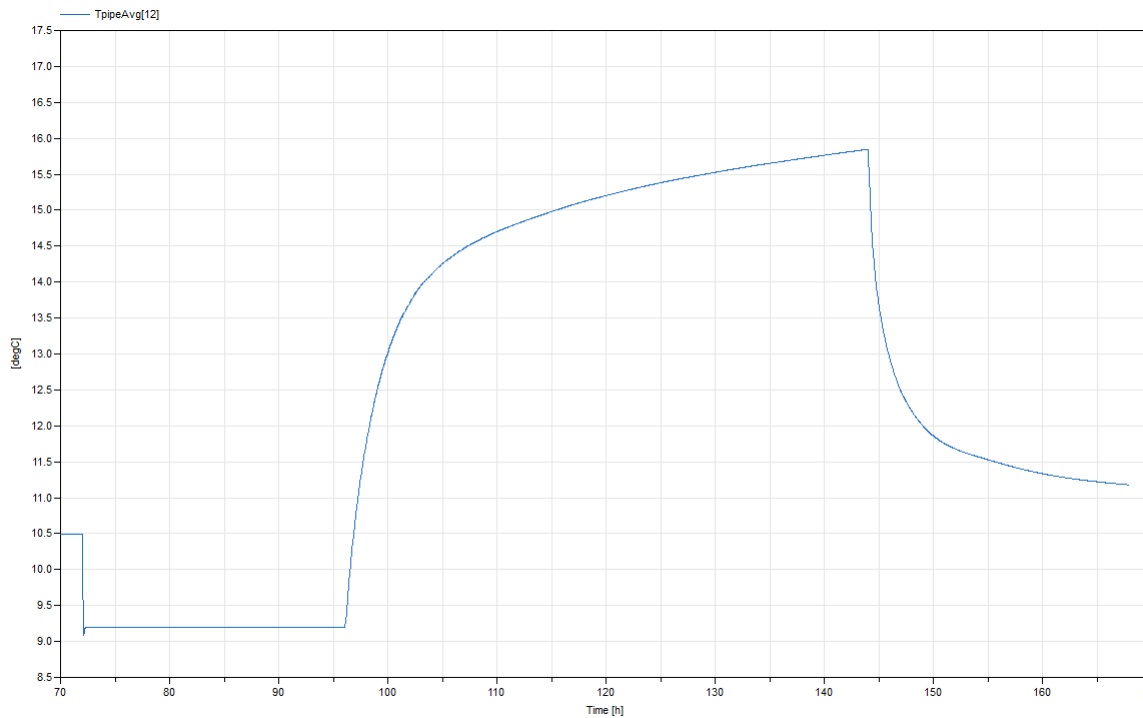


FIG. 67: Average temperature of the two pipe segments in segment 12 as a function of simulation time in Dymola.